Hamburg University of Technology

Institute for ship structural design and analysis (M-10)

Project thesis

Analysis of a FEM-model for measurements of ice loads on a ship's hull with strain gauges

B.Sc. Angelo Mario Böhm

First auditor: Prof. D.Sc. (Tech.) Sören Ehlers
Secound auditor: M.Sc. Hauke Herrnring and M.Sc. Jan M. Kubiczek

September 25, 2018

Contents

List of Figures

List of Tables

1. Declaration of Academic Integrity

I, *Angelo Mario Böhm* (Student of Naval Architecture and Ocean Engineering at Hamburg University of Technology, student number 21266467) hereby confirm that the present project's thesis on

> *Analysis of a FEM-model for measurements of ice loads on a ship's hull with strain gauges*

is solely my own work and that if any text passages or diagrams from books, papers, the Web or other sources have been copied or in any other way used, all references - including those found in electronic media - have been acknowledged and fully cited.

Hamburg, September 25, 2018

Angelo Mario Böhm

2. Abstract

The shipowner of the *HLL Rio de Janeiro* is interested in instrumenting the ship for ice load measurements in order to get a better knowledge about the ice-structure interaction on the ship's hull. The availability of several full-scale measurements in ice-covered waters is limited which is why future full-scale measurements are scientifically appreciated. The measurement of shear strains on the frame with strain gauges is chosen for the measurement set up. From the shear strains the ice load will be determined with the help of an influence coefficient matrix. In order to determine this load-strain relation of the instrumented section, a finite element analysis of this section will be conducted.

First of all, the instrumented section has to be chosen. The grommet store is picked for the investigation since this room suits the needs of a strain gauge measurement most. Besides, the room is located portside in the bow area. Afterwards the grommet store will be designed in a CAD program. In order to keep the calculation time as short as possible, a 2D surface model will be designed instead of a 3D solid model. In addition the structure will be idealized in some places. After the surface model has been created, the geometry and material data are entered. As usual for a structural analysis, boundary conditions and the loads have to be applied. The ice load is taken from the *FINNISH-SWEDISH ICE CLASS RULES* (FSICR) [19] since the *HLL Rio de Janeiro* was built in 2009. The structural analysis shows confident results, which means that the taken steps for the investigation were admissible. With the unit load principle the influence coefficient matrix is calculated using the FEM-model. This matrix shows the load-strain relation of the modeled section. In order to verify the calculated influence coefficient matrix a calibration test is suggested.

In this thesis, the steps to create the 2D surface model, the assumptions made, the theory behind them, the used measurement setup and the deviations from reality are further explained. At the end there is a recommendation for further investigations of this kind.

3. Introduction

Ships operating in ice-covered waters experience intense loads from ice. In order to investigate the ice-structure interaction of the *HLL Rio de Janeiro*, the shipowner is interested in conducting full-scale measurements of the ice loads on the *HLL Rio de Janeiro*. This thesis deals with an analysis of a finite element model of the *HLL Rio de Janeiro* for measurements of ice loads on the ship's hull using strain gauges. The author recommends the following reports, which deal with full-scale measurements of ice loads on ships [6], [7] and [17]. Mainly there are two different approaches to measure ice-induced loads on a ship's hull. One is the indirect structural strain measurement and the other is the direct measurement of the contact pressure or load. Firstly, with direct structural strain measurement the ice load acts directly on the system and can therefore be damaged quickly and secondly, the measurement setup is far more complicated and not necessarily suitable for long-term measurements. In addition, there exist mainly the two following strategies for indirect strain gauge measurement of ice loads on a ship's hull. The first strategy is the measurement on the plate between the frames, which was conducted e.g by [9]. The second strategy is the measurement on frames with strain gauges at the end of the frame, close to the next higher supporting structure as seen in [18], or distributed along the frame, see [8].
In this thesis the indirect structural strain measurement will be described and it focuses on the second strategy with strain gauges at the end of the frame, because with this method the vertical direction is resolved better. One can imagine that the rolling and trimming of the ship during ice breaking as well as ramming have a big influence on the impact area in the vertical direction. In the indirect method, the strains are measured from the frame and the external loading is determined from the load-strain relation of the built structure which is determined by a finite element analysis (FEA). After the analysis the strain gauges can be calibrated to measure the ice induced loads. It is recommended to verify the results through a calibration pull with a hydraulic press or by pressing with a tug. The analysis of the FEM model will be based on the ship *HLL Rio de Janeiro* where only a section of interest will be modeled. *HLL Rio de Janeiro*, previously called *BELUGA HOUSTON*, IMO 9424546, is a general cargo ship with an ice class to navigate through the harsh ice conditions in the Baltic Sea. Ships with an ice class have an additional level of strengthening as well as other arrangements that enable a ship to navigate through sea ice. This thesis addresses the FSICR from 2008 [19]. The *HLL Rio de Janeiro* was built in 2009, which is the reason why no current version will be considered in the first place. At the end of the analysis a recommendation will be given on where to attach the strain gauges on the ship's hull taking the assumptions made into consideration. With such a measurement system on board it is possible to determine the ice loads. [16] wrote in his dissertation about the uncertainties in the measurement of ice-induced loads on the hull. The author hereby refers to this literature. The measurement system can be understood as a decision making tool for the owner, in terms of routening and ship or ice class choice. In the following table the general data, the dimensions and the tonnage of the ship are given.

Table 1: General data, dimensions and tonnage

Name	HHL Rio de Janeiro
Call Sign	CQIG5
IMO	9424546
Built	2009
Yard	Hudong
Type	Multi Purpose Heavy Lift Vessel Strengthened for heavy cargoes and grab fitted
Class	GL + 100 A5 E3 (Ice Class)
LOA	168.68 m
Beam	25.20 m
Depth Moulded	13.85 m
DWT	20 100 mt on 9.50 m (SSW)

4. Approach

This section explains what approach is used and why certain decisions have been made, starting with the section of interest which is the grommet store at the portside of the ship. The top view of *HHL Rio de Janeiro* is shown in Figure 1. The room R4 bordered in red is the section of interest of which the FEM analysis will be conducted.

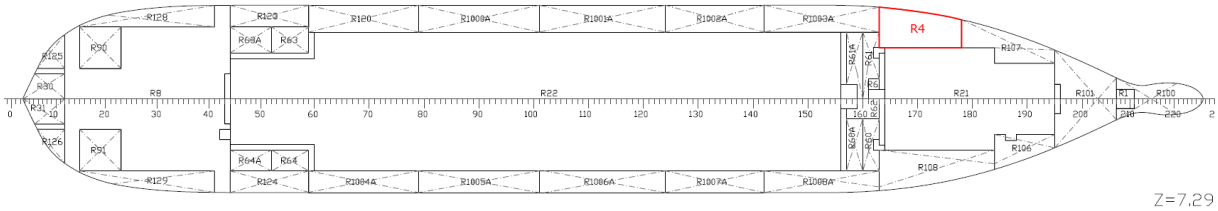

Figure 1: The top view of HHL Rio de Janeiro, $z = 7.29$ m

This room suits the needs of a strain gauge measurement most, since it is a room near the outer shell but is not a tank. Since the measuring system requires some electrical circuits and waterproof protection is too demanding for those, the room to be instrumented should not be a tank and preferably contain as little humidity as possible. Besides, the room has a good accessibility for the future attachments. In order to create a model that can be analyzed in a reasonable amount of time, only this section is considered. In addition, when enough structure is modeled to sufficiently move the boundary effects away from the area of interest, there is no benefit in modeling a greater area of the ship structure. The expected results of the area of interest will remain nearly the same with a reduction of the calculation time. The model is build up from frame 163 to frame 178, 2.40 m from the Baseline to the top and from 6.88 m off the Centerline to the outer shell. The surface-model of the section of interest which emerged from the 2D drawings is created in *Inventor Professional 2018* (CAD). Missing drawings of frames are interpolated. Although *Inventor Professional 2018* is capable of finite element analysis the surface-model is imported into *ANSYS 18.2* (CAE) where the analysis will be conducted. For the import, the common file format *STEP* will be used. Subsequently, the *STEP* file is integrated into *ANSYS 18.2 Workbench* and is opened in the *Design Modeler* tool. After opening the *STEP* file in the *Design Modeler* the geometrical model can be edited in *ANSYS 18.2 APDL*. From here, the surface-model will be build up into the FEM-model and subsequently used for the investigation.

5. Tools and Methods

This section contains the, within this project thesis, used tools and methods. The capabilities of the following tools are highlighted briefly. Computer Aided Design (CAD) is generally used for the creation of three dimensional models. In contrast to Computer Aided Engineering (CAE), CAD is used only for designing purpose. CAE on the other hand provides a set of methods, that can elaborate the performance of structures in different environments. In this specific case, the deflections and stresses of the ship hull need to be elaborated. For this purpose CAE using finite element method (FEM), is used for calculating the structures performance under a certain load setup.

5.1. CAD

In this subsection the used program *Inventor Professional 2018* (CAD) will be described and it will be explained why it was used. *Inventor Professional 2018* offers three dimensional mechanical design, documentation and product simulation developed by *Autodesk*. *Inventor Professional 2018* includes a free-form modeling tool which is very suitable for creating the shell of the section of interest. The advantage from *Inventor Professional 2018* is, that free-form surfaces can be created intuitively and true to scale by using the existing drawings.

5.2. CAE

In this subsection the FEM will be outlined briefly, the used program *ANSYS 18.2* will be described and it will be explained why it was used. For more details regarding the finite element method the author suggest the following literature [3]. For practical problems of structural analysis, for example an analysis of the ice-structure interaction of a ship's hull, it is impossible to define a global approximation. For various problems a global approximation can be created only under rough assumptions and a limited usability. The concept behind FEM is to split the global problem in finite computational domains, so called finite elements, where a local approximation is introduced which satisfies the local structural needs. An analysis of a structural problem with finite element method starts with the discretization of the computational domain with finite elements using a mesh generator. In order to get results which corresponds with the actual structural behavior, the computational domain have to be discretized with finite elements which suites the mechanical model of the actual structure. Here, the structural elements, beams and shells will be used.
The quality of the solution goes hand in hand with the discretization. That means, the solution can be improved among other things by refining the mesh. There are other methods to improve the solution, like using high-order shape functions, but this will not be discussed further. For more information regarding the improvement of FEM solutions the author refers the following literature [2]. The downside is obviously that a finer mesh results in more local computational domains and so in more computational time. After applying a proper mesh the structural boundary conditions have to be considered. The boundary conditions will be applied on the nodes of the finite elements. Since the

boundary conditions have an impact on the accuracy of the solution they should also fit as good as possible the mechanical needs of the problem. Otherwise it is recommended to enlarge the model to shift the boundary effects away from the area of interest. When the finite element mesh has been generated, *ANSYS 18.2* assembles the elements contribution to the global stiffness matrix. With the boundary conditions and a global load vector the nodal displacement can be calculated, by solving the global system of equation.
In order to maintain a consistent mathematical notation all matrices and vectors will be bold. Thus, it can be distinguished between scalar symbols and matrix or vector symbols.

$$\boldsymbol{K}\boldsymbol{u} = \boldsymbol{F} \tag{1}$$

The global stiffness matrix $\boldsymbol{K}$ is defined by the materialistic properties and geometrical data. The global load vector $\boldsymbol{F}$ defines the applied loads on the elements. As a result, the vector $\boldsymbol{u}$ is calculated and finally shows its displacement.

$$\boldsymbol{u} = \boldsymbol{F}\boldsymbol{K}^{-1} \tag{2}$$

The structural analysis will be conducted with the engineering simulation and three dimensional design software *ANSYS 18.2*. It enables to solve complex structural engineering problems and to help in the design decision-making process. *ANSYS 18.2* is capable of computing nonlinear behavior of structures which are composed of nonlinear material as is the case here. It should be mentioned, that any decent FEM program could be used for the purpose of this project thesis, but *ANSYS 18.2* was chosen for licensing reasons.

6. Structural idealization

To find a good compromise between calculation accuracy and calculation time, the structure should be idealized at suitable locations. Structural idealization means avoiding small line elements and high aspect ratios. Small line elements result in a finer mesh in an unwanted manner and high aspect ratios can result in an interpolation error of unacceptable magnitude [10]. Besides, highly skewed elements have to be avoided because highly skewed elements can decrease the accuracy of the solution. The skewness can be understood as the difference between the shape of an actual element and the shape of an equilateral element of equivalent volume or area, depending on the viewed dimension. Optimal quadrilateral meshes will have angles close to 90 degrees. In addition, idealization near the boundary condition is more admissible than near the outer shell, where the load is applied, because as mentioned in Section 4 enough structure is modeled to move the boundary effects away form the area of interest. The boundary condition will be applied at the Frame 163 and 178, at the plane 6.88 m off the centerline and at the plane 2.40 m above the Baseline, so everything near these planes can be idealized more. The outer shell is the most important and complex structure of the ship regarding the ice load and the modeling process, which is why this part should be modeled as close to reality as possible. In Figure 2 a supporting structure at Frame 164 is depicted. The red lines emerged from the original drawings. The yellow lines are the edges of the modeled surfaces in *Inventor Professional 2018*. In order to avoid highly skewed elements some edges from cutouts are modeled as triangles.

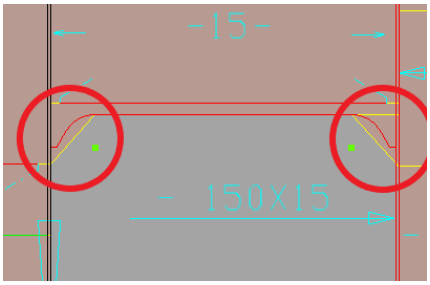

Figure 2: Supporting structure at Frame 164

As can be seen in Figure 2, marked in red circles, the shape of the surface differs from the original drawings in order to avoid small line elements and highly skewed elements. With this execution two small line elements are avoided on each side. As mentioned before the quality of the solution depends on the mesh, among other things. If the mesh is finer, the solution should converge to the exact solution at the expense of the calculation time. However, unnecessary finer local meshes increase the calculation time without contributing to the accuracy of the global solution to some extend. In many cases small line elements, highly skewed elements and high aspect ratios could not be avoided because the local geometry could not be modeled differently at these particular locations. So the only way to reduce the number of elements with a high skew or a high aspect ratio is to re-mesh these particular locations with other parameters like element size for example.

7. Development of the finite element model

In this section the development of the finite element model will be presented. It also deals with what to consider when dealing with *Inventor Professional 2018* and *Ansys 18.2*, which problems arose and how they were solved. First of all it is important to mention that SI units cannot be given to *Ansys 18.2*. In order to get results with the right magnitude it is highly suggested to give the program consistent units through using values with consistent magnitudes. In the table below, the units are given, which the analysis strictly adhered to.

Table 2: Used units in *Ansys 18.2*

Mass	Length	Time	Force	Stress	Energy
kg	m	s	N	Pa	Joule

All results that originate from the analysis correspond to these units. After importing the geometry from *Inventor Professional 2018* to *Ansys 18.2* the geometry has to be checked. Here the first problem occurs. When modeling plates with surfaces in *Inventor Professional 2018* you give the program, by clicking, only the node information. In case of a quadrilateral the surface will be created after creating the 4th node. The problem is that nearby surfaces do not share the edge, or rather, the line information. As a matter of fact the *stitch* function of *Inventor Professional 2018* could not solve this problem either. After the import it occurred that there were many surfaces with perhaps the same node information but yet not with the same line information. Many overlapping lines had to be removed as well overlapping keypoints, since differences occurred in the micro millimeter range through clicking. In Figure 3 the problem with the overlapping lines is depicted.

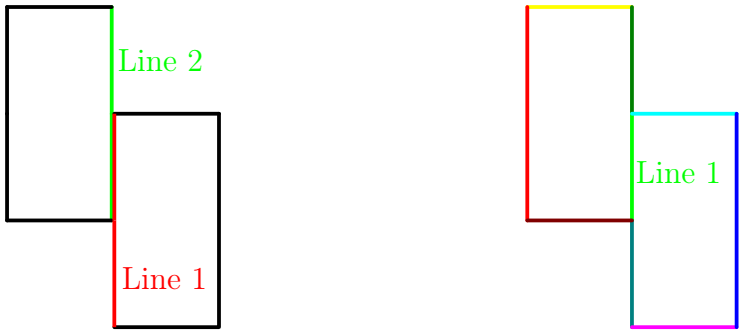

Figure 3: Example: Left overlapping lines; Right plates share line No. 1

In contrast to the left example the right example shows how it should look like when it is done correctly. Since there is no current possibility in *Inventor Professional 2018* to do so, the reworking is done in *Ansys 18.2*. When nearby surfaces do not share the same nodes or lines as is shown in Figure 3 in the left example, the surfaces are not connected with each other. To ensure that the reworking is done precisely a modal analysis is conducted.

The modal analysis shows the characteristic dynamic behavior of the structure. It should be mentioned that the modal analysis is only conducted for the purpose of identifying unconnected surfaces. As depicted in the figures below, 100 modes have been checked in a frequency range from 0 to 1000 Hz, which are realistic values for this type of analysis. The settings of the conducted modal analysis is presented in Figure 4 and Figure 5.

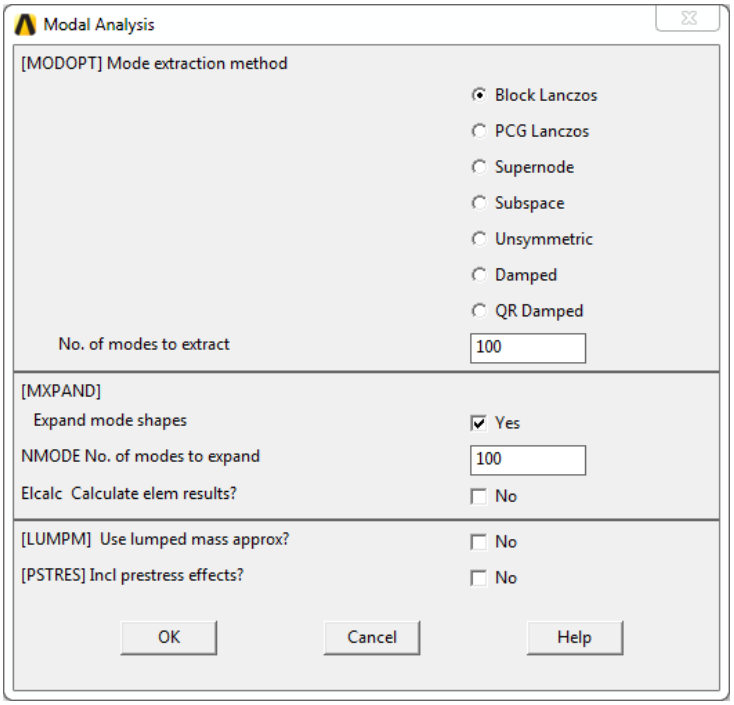

Figure 4: Modal analysis settings part 1

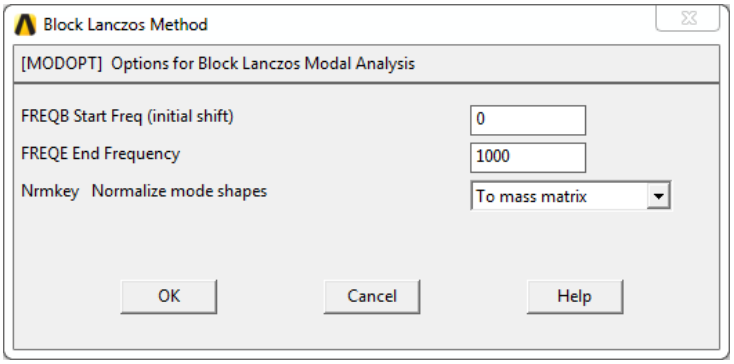

Figure 5: Modal analysis settings part 2

With the modal analysis the remaining unconnected surfaces were identified and fixed afterwards.

7.1. Mechanical model

After ensuring the correctness of the surface model the material data and sectional data can be implemented. Basically two element types are used. Shell elements, so called *shell181* in *Ansys 18.2*, for all plates and beam elements, so called *beam188* in *Ansys 18.2*, for all stiffeners. Since the accuracy of the solution is primarily governed by fundamental assumptions of the theories behind the used element types, these theories will be described here briefly.

Beam188 is suitable for analyzing slender to moderately stubby or thick beam structures. In addition shear deformation effects are included. Besides, the element is a linear 2-node beam element with six degrees of freedom at each node. The degrees of freedom at each node include translations in x, y, and z direction, and rotations about the x, y and z-axes [13]. The *beam188* element is based on the *Timoshenko beam theory*. Following assumptions are made in the *Timoshenko beam theory* [4]:

1. The longitudinal axis of the unloaded beam is straight.
2. All applied loads act transverse to the longitudinal axis.
3. All deformations and strains are small.
4. Hooke's law can be used to relate stresses and strains.
5. Plane cross sections, which are initially normal to the longitudinal axis, will remain plane after deformation.

Out of this assumptions following equations of motion emerge:

$$\frac{\mathrm{d}^2}{\mathrm{d}x^2}\left(EI\frac{\mathrm{d}\varphi}{\mathrm{d}x}\right) = q(x) \tag{3}$$

$$\frac{\mathrm{d}w}{\mathrm{d}x} = \varphi - \frac{1}{\kappa AG}\frac{\mathrm{d}}{\mathrm{d}x}\left(EI\frac{\mathrm{d}\varphi}{\mathrm{d}x}\right) \tag{4}$$

Where E is the Young's modulus, A is the cross section area, I is the second moment of area, G is the shear modulus, $q(x)$ is a distributed load and κ is the Timoshenko shear coefficient. The combination of the two equation above, results to the following equation of motion for a homogeneous beam with a constant cross section:

$$EI\frac{\mathrm{d}^4w}{\mathrm{d}x^4} = q(x) - \frac{EI}{\kappa AG}\frac{\mathrm{d}^2q}{\mathrm{d}x^2} \tag{5}$$

In order to get the *weak form*, which is needed for the finite element formulation, the equation above is multiplied by a test function. This test function has to satisfy the boundary conditions. After applying the test function the equation is integrated over the whole domain through integration by parts which leads to the *weak form*. The *Timoshenko bar theory* extends the classical *Euler-Bernoulli bar theory* by an additional spatial derivation of the second degree, as it can be seen in Equation 3. Thus the Bernoulli assumption

that the cross-section of a beam remains perpendicular to the beam axis even after deformation is no longer fulfilled. For visualizing purpose, the differences between the main assumptions of these two theories are depicted in Figure 6. The stiffness of the beam is reduced by allowing additional shear deformation. This results in higher deformations and lower natural frequencies which is good for a more realistic approach.

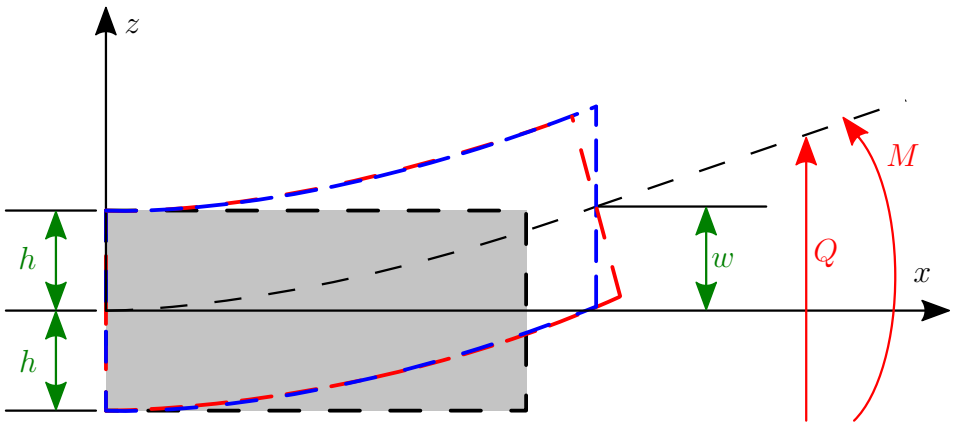

Figure 6: Deformation of a *Timoshenko beam* (blue) versus of an *Euler-Bernoulli beam* (red)

Shell181 is suitable for analyzing thin to moderately-thick shell structures and it is also well-suited for linear, large rotation, and/or large strain nonlinear applications [14]. Ideally it is a four-node element, but the model is also capable of handling three-node elements. Furthermore each node has six degrees of freedom. Translations in the x, y and z directions and rotations about x, y and z-axes are possible. In reality each structure is three-dimensional but it is possible to introduce assumptions that lead to a reduction in dimensions. The *Reissner-Mindlin plate theory* is a classical example of a dimensional reduction of the three-dimensional elastostatic equation for thin and moderately thick plates. For it one dimension, the thickness, has to be small compared to the other two dimensions and then the structure can be classified as thin-walled. Moreover the *Reissner-Mindlin plate theory*, which is the theory behind the *shell181* element, is also accounting for transverse shear strains. In this theory a mid-surface is introduced and the displacements are related to this mid-surface. The theory assumes that normals to the mid-surface remain straight lines after deformation. Due to these assumptions the 1D analogon of the *Reissner-Mindlin theory* is the *Timoshenko beam*. A reason why the elements are compatible with each other. Following equations, which are used behind the *shell181* element, were elaborated based on the Figure 7. The Figure 7 shows a plate with thickness t, which is subjected to a surface load $q(x, y)$ acting in the z-direction. The *Reissner-Mindlin plate theory* makes the following assumptions so the original three-dimensional problem is reduced into a two-dimensional problem:

1. Normals to the mid-surface remain straight lines, but not necessarily normals after deformation.

2. The plate has a moderate thickness t, and the deflection w is independent of z, so that $u_z(x, y, z) = w(x, y)$ holds.

3. Points on the mid-surface are deformed in the z-direction only.

4. Stresses perpendicular to the mid-surface are disregarded, $\sigma_{zz} = 0$.

Resulting in the following equations:

$$0 = \frac{\partial M_x}{\partial x} + \frac{\partial M_{xy}}{\partial y} - Q_x \tag{6}$$

$$0 = \frac{\partial M_y}{\partial y} + \frac{\partial M_{xy}}{\partial x} - Q_y \tag{7}$$

$$0 = \frac{\partial Q_x}{\partial x} + \frac{\partial Q_y}{\partial y} - q(x, y) \tag{8}$$

With the bending moments M_x, M_y and the twisting moments $M_{xy} = -M_{yx}$ and the shear forces Q_x, Q_y. In order to get the *weak form*, which is needed for the finite element formulation, the Equations 6, 7 and 8 are multiplied by a test function. This test function has to satisfy the boundary conditions. After applying the test function the equations are integrated over the whole domain through integration by parts which leads to the *weak form*. The problem with the *Reissner-Mindlin* plate elements is, that it leads to artificial stiffening effects when the plate becomes increasingly thinner. This effect, so called *shear locking*, leads to the problem, that its totally underestimates the deformation of the plate [3]. An way to overcome *shear locking* is to use a so called *reduced integration*, where the elements are under-integrated. *Ansys 18.2* is capable of using this method. For more information the author makes a reference to the following literature [3].

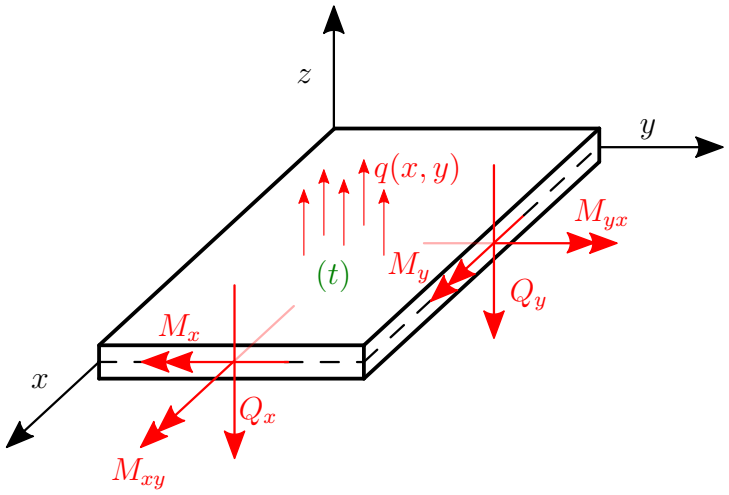

Figure 7: Sign convention of the *Reissner-Mindlin plate theory*

The applicability of shell theory and of the beam theory in such cases is best understood by using a comparable solid model.

7.2. Material model

A brief description of the theory behind the material model is given to support the made decisions. As well as to give the reader a better understanding for the analysis part, for instance for the evaluation of the *von Mises stresses* of the structure. In order to create model which satisfies the actual material behavior of the structure, but as with the approach of the structural idealization does not unnecessarily increase the calculation time, a bilinear material model is used. That is, that the model is decomposed in two linear models. In the table below the various materials, which were used on the ship, more precisely in the section of interest, are listed.

Table 3: Material data

Name	Young's modulus [GPa]	Yield strenght [MPa]	Poisson's ratio [-]
A	206	235	0.3
AH36	206	360	0.3
DH36	206	235	0.3
EH36	206	235	0.3

Metals, among many other materials, have two major characteristics when they are under a certain stress range. These two characteristics are the elasticity and the plasticity. When the stresses does not exceeding the yield strength σ_Y, point A in Figure 8, the material can fully recover to its initial shape upon unloading.

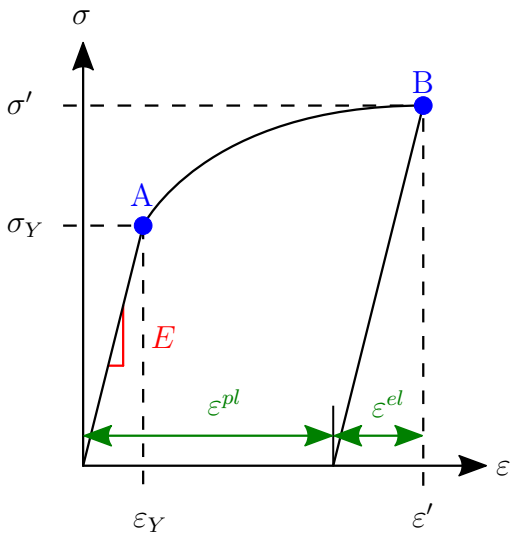

Figure 8: Typical stress-strain curve

In this elastic area the deformation is proportional to the load however the elastic strains tend to be small. The elastic behavior of metals is most commonly described by the stress-strain relationship of *Hooke's Law*:

$$\boldsymbol{\sigma}_Y = E\boldsymbol{\varepsilon}_Y \tag{9}$$

Exceeding the yield strength leads to nonrecoverable plastic deformation, point B in Figure 8. After unloading the material the elastic area of the total strain will be recovered but a permanent deformation remains in the material due to the plastic strain area, as it is depicted in Figure 8. Besides, it can be observed that the stress at point B is lager than in point A, which is due to hardening. The constitutive models for elastic-plastic behavior start with a decomposition of the total strain into elastic and plastic parts and using separate constitutive models for each part [12], [21]. The elastic constitutive model is the *Hooke's Law* whereby the plastic constitutive models are divided into the following subjects:

- The yield criterion that defines the material state at the transition from elastic to elastic-plastic behavior.
- The flow rule that determines the increment in plastic strain from the increment in load.
- The hardening rule that gives the evolution in the yield criterion during plastic deformation.

The following explanation of the yield criterion is based on [3]. The *von Mises yield criterion* will be used within the scope of this thesis. It suggest that yielding begin when the second deviatoric stress invariant J_2 reaches a critical value. The *von Mises stress* can be obtained by an additive decomposition of the stress tensor. The stress tensor in index notation is defined as follows:

$$\boldsymbol{\sigma} = \begin{bmatrix} \sigma_{11} & \sigma_{12} & \sigma_{13} \\ \sigma_{21} & \sigma_{22} & \sigma_{23} \\ \sigma_{31} & \sigma_{32} & \sigma_{33} \end{bmatrix} \tag{10}$$

The indices 1, 2, 3, correspond to the directions x, y, z, respectively. The stress tensor can be decomposed as follows:

$$\boldsymbol{\sigma} = \frac{1}{3}(\mathrm{tr}\boldsymbol{\sigma})\boldsymbol{I} + \mathrm{dev}\boldsymbol{\sigma} \tag{11}$$

With the *mean normal stress* term

$$\sigma_{\mathrm{m}} = \frac{1}{3}(\mathrm{tr}\boldsymbol{\sigma}). \tag{12}$$

And the so called *stress deviator* term

$$\boldsymbol{s} = \mathrm{dev}\boldsymbol{\sigma} = \boldsymbol{\sigma} - \frac{1}{3}(\mathrm{tr}\boldsymbol{\sigma})\boldsymbol{I}. \tag{13}$$

Therefore in matrix notation follows:

$$\begin{bmatrix} \sigma_{11} & \sigma_{12} & \sigma_{13} \\ \sigma_{21} & \sigma_{22} & \sigma_{23} \\ \sigma_{31} & \sigma_{32} & \sigma_{33} \end{bmatrix} = \begin{bmatrix} \sigma_{\mathrm{m}} & 0 & 0 \\ 0 & \sigma_{\mathrm{m}} & 0 \\ 0 & 0 & \sigma_{\mathrm{m}} \end{bmatrix} + \begin{bmatrix} \sigma_{11} - \sigma_{\mathrm{m}} & \sigma_{12} & \sigma_{13} \\ \sigma_{21} & \sigma_{22} - \sigma_{\mathrm{m}} & \sigma_{23} \\ \sigma_{31} & \sigma_{32} & \sigma_{33} - \sigma_{\mathrm{m}} \end{bmatrix} \tag{14}$$

In order to get the invariants for the stress deviator the determinant of the coefficient matrix

$$\begin{vmatrix} \sigma_{11} - \sigma_{\mathrm{m}} & \sigma_{12} & \sigma_{13} \\ \sigma_{21} & \sigma_{22} - \sigma_{\mathrm{m}} & \sigma_{23} \\ \sigma_{31} & \sigma_{32} & \sigma_{33} - \sigma_{\mathrm{m}} \end{vmatrix} = 0 \tag{15}$$

has to vanish. Resulting in the following three invariants:

$$J_1 = \mathrm{tr}\ \boldsymbol{s} = (\sigma_{11} - \sigma_{\mathrm{m}}) + (\sigma_{22} - \sigma_{\mathrm{m}}) + (\sigma_{33} - \sigma_{\mathrm{m}}) = 0 \tag{16}$$

$$J_2 = \frac{1}{2}\left((\mathrm{tr}\ \boldsymbol{s})^2 - \mathrm{tr}\ (\boldsymbol{s}^2)\right) = -\frac{1}{2}\mathrm{tr}\ (\boldsymbol{s}^2) \tag{17}$$

$$J_3 = \det \boldsymbol{s} \tag{18}$$

With the second invariant the *von Mises equivalent stress* can be obtained. It reduce the three dimensional stress state to one dimensional stress state.

$$\sigma_{vM} = \sqrt{-3J_2} = \sqrt{\frac{1}{2}\left[(\sigma_1 - \sigma_2)^2 + (\sigma_2 - \sigma_3)^2 + (\sigma_3 - \sigma_1)^2\right]} \tag{19}$$

The *von Mises stress* is used to predict yielding of materials under complex loading from the results of uniaxial tensile tests. The *von Mises stress* satisfies the property where two stress states with equal distortion energy have an equal *von Mises stress* [20]. It can be understood as a common decision making tool for an engineer.
To move on to the flow rule. The following explanation is based on [21]. The flow rule, for most metals, gives the direction of flow by the partial derivative of the flow condition with respect to the deviatoric stresses.

$$\mathrm{d}\boldsymbol{\varepsilon}^{pl} = \lambda \frac{\partial f}{\partial \boldsymbol{s}} \tag{20}$$

The equation above describes the evolution of the deviatoric plastic strains. The direction of plastic flow is given by $\frac{\partial f}{\partial \boldsymbol{s}}$ and λ is a scalar which determines the size of the plastic strain increment. In order to get an elastic-perfectly plastic material model, which is used within the scope of this thesis, λ is to be chosen as zero.
Last of all the hardening rule has to be chosen. The change in the yield criterion due to loading is called hardening. There are two classical models of elasto-plasticity. On the one hand you have isotropic hardening, where the flow surface expanses, and on the other hand you have the kinematic hardening, where the origin of the flow surface shifts. Since an elastic-perfectly plastic material model is chosen, which does not account for hardening effects, it does not matter what criterion is chosen in *Ansys 18.2*. Here, an isotropic hardening rule is picked.

To summarize, the plastic behavior is typically characterized by the slope of the stress-strain curve beyond the yield point that shows the degree of hardening. Hardening is an effect which occurs at cycle loading and unloading beyond the yield stress. It is distinguish between kinematic an isotropic hardening. Plastic deformations are not expected within the scope of this thesis due to the expected low ice induced loads but for further analysis it is recommended to choose material models with plastic properties. In order to get conservative results an elastic-perfectly plastic material model, which does not account for hardening effects, will be used. A stress-strain curve of an elastic perfectly-plastic material model is depicted in the following Figure 9.

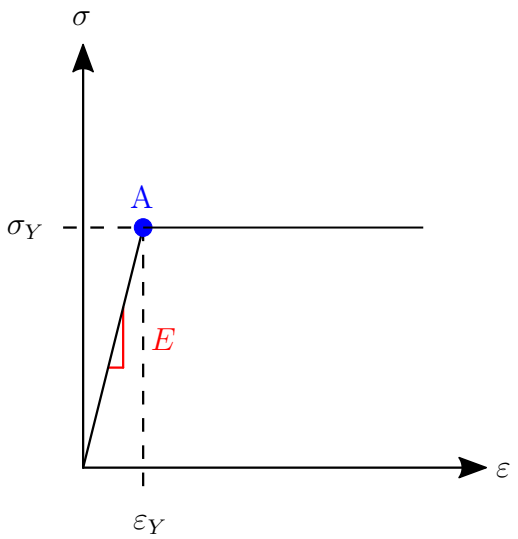

Figure 9: Stress-strain curve of an elastic perfectly-plastic model

As it can be seen no hardening effects occur in this model.

7.3. Boundary condition

The boundary condition will be applied at the nodes of the elements. For this purpose four planes will be defined as follows.

Table 4: Boundary planes

	Plane 1	Plane 2	Plane 3	Plane 4
at	$x = 0$ m	$x = 11.1$ m	$z = 0$ m	$y = 0$ m

Basically, Plane 1 describes all nodes at Frame 163 and Plane 2 describes all nodes at Frame 178. Plane 3 describes all nodes at 2.40 m above the baseline, at the double bottom and at last Plane 4 describes all nodes at 6.88 m of the centerline, portside. The following boundary conditions are used for the investigation.

Table 5: Boundary condition case

Plane 1	Plane 2	Plane 3	Plane 4
$u_x = u_y = u_z = 0$	$u_x = u_y = u_z = 0$	$u_x = u_y = u_z = 0$	$u_x = u_y = u_z = 0$
$\varphi_x = \varphi_y = \varphi_z = 0$	$\varphi_x = \varphi_y = \varphi_z = 0$	$\varphi_x = \varphi_y = \varphi_z = 0$	$\varphi_x = \varphi_y = \varphi_z = 0$

The assumption is that near the boundary conditions the stresses will be much higher compared to reality, since the large bending moments are inherent for a rigid clamp boundary condition. At the same time it is expected that the displacement will be much greater in areas far away from the boundary conditions. More precisely, the largest displacement is expected at the center of the applied force. Through the chosen case it is possible that plastic deformation occurs because of the high stresses at the boundary conditions, though in reality plastic deformation should not occur at this magnitude of load. To get a better understanding of the influence of the boundary effects on the global solution, various boundary conditions can be applied. For a more precise analysis, the stiffness of the surrounding structure should be applied by mechanical springs at the places of the boundary conditions instead of applying the boundary conditions in the form of displacement restrictions. The assumed boundary condition is sufficient to evaluate the structural behavior.

7.4. Ice loads

The *HLL Rio de Janeiro* was built in 2009, which is the reason why the ice loads will be applied according to the FSICR [19] from 2008. Mainly the focus lies on the Section "4.2 Ice load" from the FSICR. The *HLL Rio de Janeiro* has an *ice class IA* which is defined as follows:

"ships with such structure, engine output and other properties that they are capable of navigating in difficult ice conditions, with the assistance of icebreakers when necessary."

For an ice-strengthened ship which operates in open sea conditions the level ice thickness shall not exceed h_0, according to the rules. The design height $h(t) = const.$ of the contact area between the ice and the structure remains at any point of time the same, although it is only a fraction of the ice thickness. The following values can be taken from the rules:

Table 6: Design height h and h_0

Ice class	h_0 [m]	h [m]
IA	0.8	0.3

To calculate the ice pressure the following formula is given:

$$p = c_d \cdot c_p \cdot c_a \cdot p_0 \text{ [MPa]} \tag{21}$$

First, p_0 the nominal ice pressure is, according to the rules, set to the following value:

$$p_0 = 5.6 \text{ [MPa]} \tag{22}$$

The factor c_d takes the influence of the size and the engine output of the ship into account and will be determined by the following formula:

$$c_d = \frac{a \cdot k + b}{1000} = 0.621 \tag{23}$$

With, k, calculated by the following formula:

$$k = \frac{\sqrt{\Delta \cdot P}}{1000} = 17.151 \tag{24}$$

Where Δ is the displacement of the ship at maximum ice class draught [t] and P is the actual continuous engine output of the ship [kW]. The ship has the following values:

$$P = 9800 \text{ [kW]} \tag{25}$$

$$\Delta = 30016.2 \text{ [t]} \tag{26}$$

Since the section of interest is a *forward* region and $k > 12$, following values will be used for a and b:

$$a = 6 \tag{27}$$

$$b = 518 \tag{28}$$

The factor c_p takes into account of the probability that the design ice pressure occurs in a certain region of the hull for the ice class in question. The section of interest is a *forward* region and it's an IA class ship, so for c_p follows:

$$c_p = 1 \tag{29}$$

c_a is a factor which takes account of the probability that the full length of the area under consideration will be under pressure at the same time. It is determined by the formula:

$$c_a = \frac{47 - 5l_a}{44};\ \text{maximum 1.0; minimum 0.6,} \tag{30}$$

In addition, l_a shall be taken as follows:

Table 7: Definition of the load length according to the FSICR from 2008

Structure	**Type of framing**	l_a [m]
Shell	Transverse	Frame spacing
	Longitudinal	2 · frame spacing
Frames	Transverse	Frame spacing
	Longitudinal	Span of frame
Ice stringer		Span of stringer
Web frame		2 · web frame spacing

This results in the following design loads:

Table 8: Load length, ice pressure and line load

Structure	l_a [m]	c_a	p [MPa]
Shell	0.37	1.000	3.478
Frames	0.37	1.000	3.478
Ice Stringer	0.74	0.984	3.422
Web frame	1.48	0.900	3.130

The interesting part of the shell is the ice belt region, since it is designed according to the rules. The ice belt region is additionally enforced and contains two ice stringers. In Table 9 the location of the applied ice loads and the corresponding load values are shown.

Table 9: Location of ice loads

Load Case No.	Category	Depths [m]	p [MPa]	Description
1	A	9.4	3.478	Between deck 10.30 m and ice-stringer 8.50 m
2	B	8.5	3.422	On ice-stringer 8.50 m
3	A	7.9	3.478	Between ice-stringer 8.50 m and deck 7.30 m
4	A	6.7	3.478	Between deck 7.30 m and ice-stringer 6.10 m
5	B	6.1	3.422	On ice-stringer 6.10 m
6	A	5.2	3.478	Between ice-stringer 6.10 m and deck 4.30 m

As it can be seen in the Table 9 there are 2 categories of load cases. In Category A the ice load is applied at the middle of the plate. In Category B the ice load is applied at the ice-stringer directly.

8. Analysis results and structural behavior

The displacements and the stresses will be depicted and described in the next subsections. Furthermore the evaluation will be based only on two load cases. The evaluation of the other load cases is not necessary, as similar structural behavior is to be expected, as long as it is a load case from the same category. The first load case is No. 3 from the Category A and the other load case is No. 2 from the Category B. Besides, the results of the analysis of all load cases are depicted in the Appendix A. In the Table 10 the different load cases are given with the maximum occurred displacement in the viewed section.

Table 10: Maximum displacement

Load Case No.	Category	u_{sum} [mm]
1	A	6.754
2	B	4.910
3	A	5.384
4	A	5.348
5	B	6.755
6	A	9.711

8.1. Displacement

In this subsection the displacement of the load case No. 3 and No. 2 will be evaluated. The load case No. 3 from Category A is chosen due to the fact that the moulded design draft of 8.10 m comes close to the depth of the load case No. 3 which is 7.90 m. One could also come to the conclusion that it would be better to apply the load on the draft of 8.10 m, but it is always a more conservative case when a load acts in the middle of a plate. At a draft of 7.90 m the load acts in the middle of the plate. The second load case, which will be evaluated, is No. 2, because it is a load case from the Category B and the load case lies closer to the moulded design draft out of the load cases from Category B. Starting with the load case No. 3, the displacement of the shell is depicted in Figure 10. More precisely, the ice belt region can be seen and the section is rotated, so that the inner structure is visible.

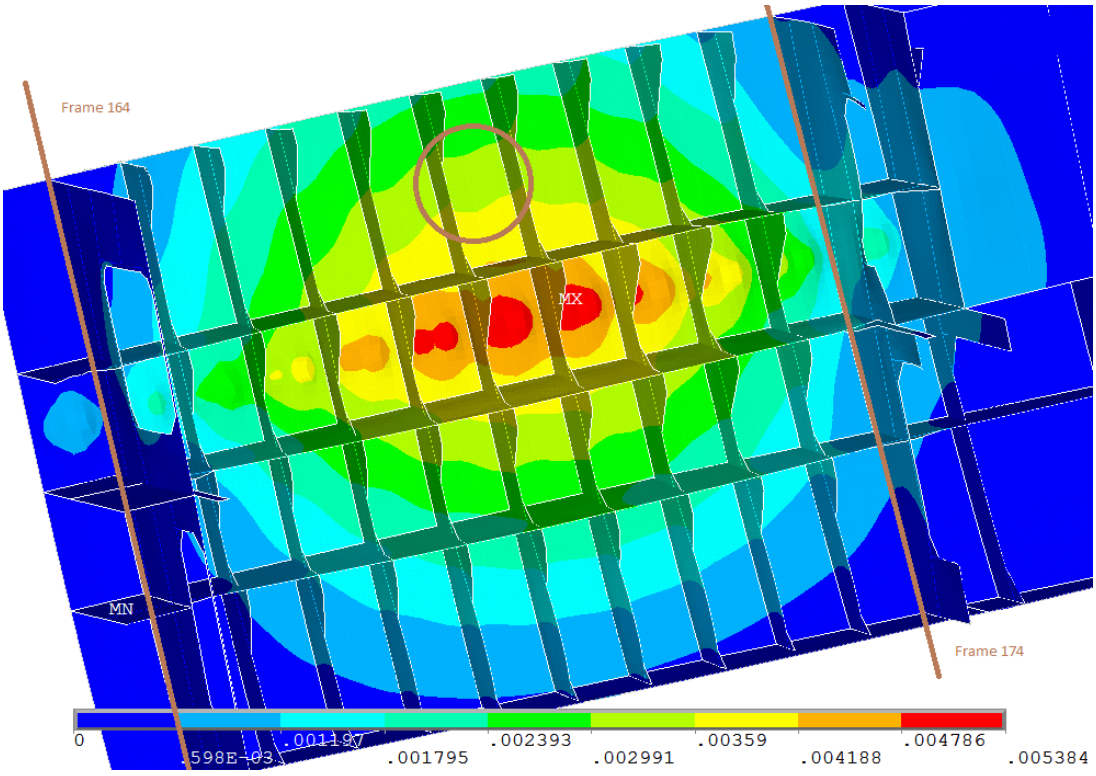

Figure 10: Displacement due to load case No. 3, ice belt region

The nodal solution of the resulting displacement is displayed. In every figure in this chapter you can see a legend in the form of a bar. This bar goes from the minimum to the maximum of the viewed mechanical value. In order to visualize the images better, the bar is divided between the maximum and minimum by different color bars equidistantly. This legend will be shown in the following figures of this chapter as described. For visualizing and orienting purposes the location of Frame 164 and Frame 174 are marked in brown. From Frame 174 on there are no web frames but rather bulkheads which makes this

particular area stiffer. This is to say, that is the reason why the displacement does not increase at the right side to the middle as fast as from the left side to the middle. It can be assumed that the stresses will behave vice versa. It can be observed that the displacement between the shells is a bit wavy. This behavior is best to see in the brown circled area. That is due to the beam elements which are lying on the lines of the model and are not visible. So the wavy appearance is justified. Apart from that, the structure behaves as expected under the encountered conditions. The maximum displacement is 5.384 mm in total and occurs between Frame 170 and 169.
Continuing with the load case No. 2, in Figure 11 the nodal solution of the resulting displacement is displayed. Besides, the ice belt region can be seen and the section is rotated, so that the inner structure is visible.

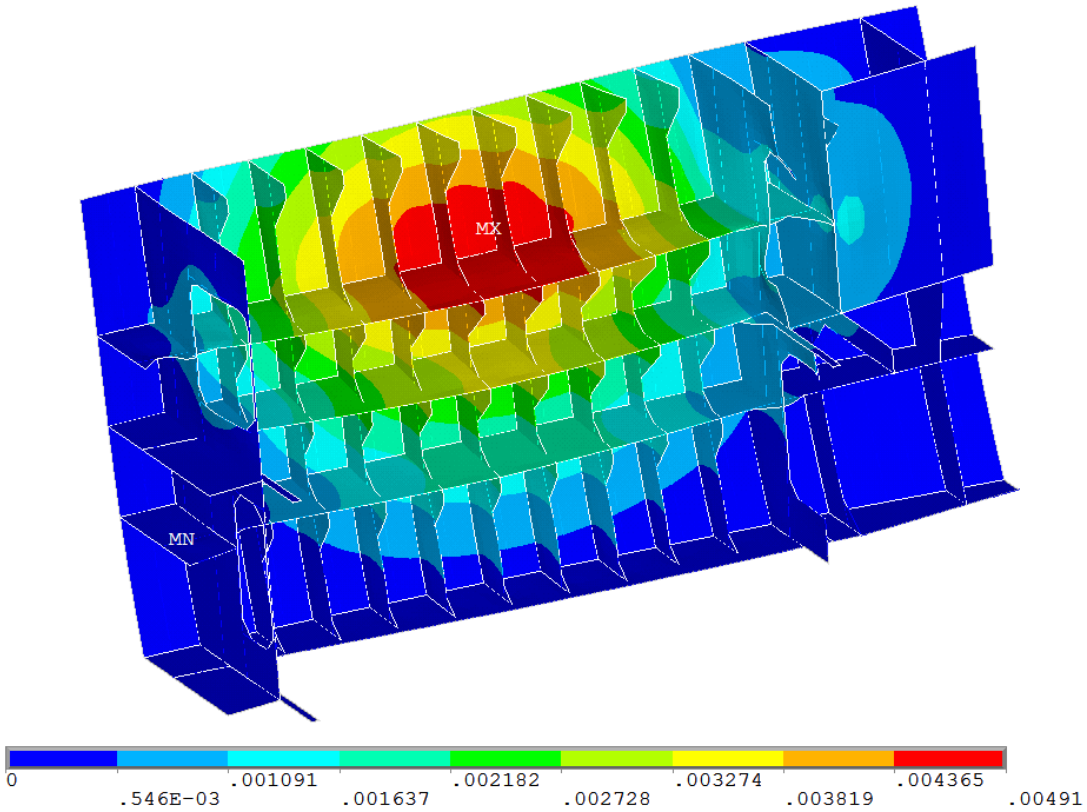

Figure 11: Displacement due to load case No. 2, ice belt region

Compared to the previous load case No. 3, in which the load is applied in the middle of the plate field, a stronger distribution of the maximum displacement can be seen. This is due to the fact that the load is better distributed by the ice-stringer. This is the reason why the ice-stringers are used in the first place. The maximum displacement is 4.910 mm in total and occurs between Frame 170 and 169. The maximum displacement here is the least of the calculated load cases. An other difference is that the maximum displacement is on the ice-stringer, which was to be expected in this Category B. The same wavy behavior is best seen at this view point.

8.2. Stresses

In this subsection the *von Mises stress* of the load case No. 3 and No. 2 will be evaluated. Starting again with the load case No. 3, the *von Mises stress* of the shell is depicted in the Figure 12.

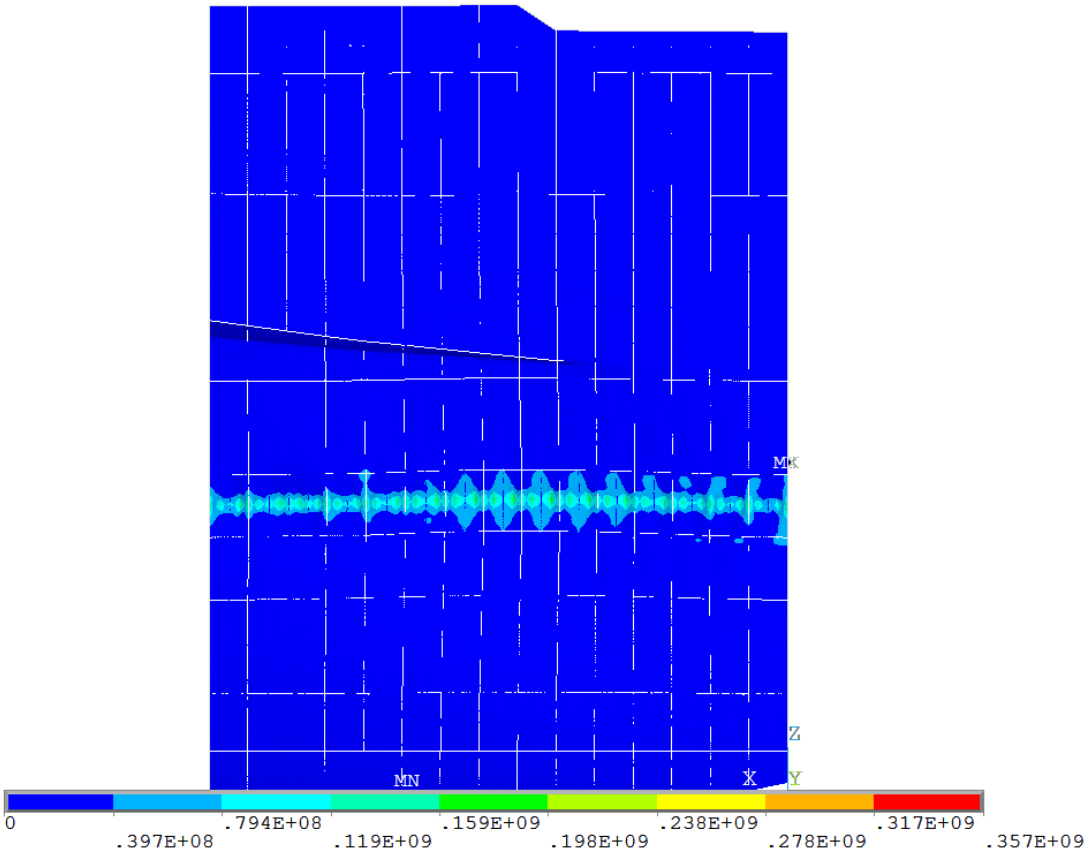

Figure 12: *von Mises stress* due to load case No. 3

Here the stiffening effect of the beams is more visible. Next to the wavy appearance it can be seen that the beams are shifting the stresses. On the one hand the stresses are reduced but on the other hand, the stresses are distributed more in vertical direction. The maximum stresses are close to the yield point, which indicates a plastic behavior. The maximum of the legend shows stresses of 357 MPa, which is near the yield strength of the AH36 material.

Going on to the Figure 13. For visualization purposes, the ice belt region is rotated, so that the inner structure is visible.

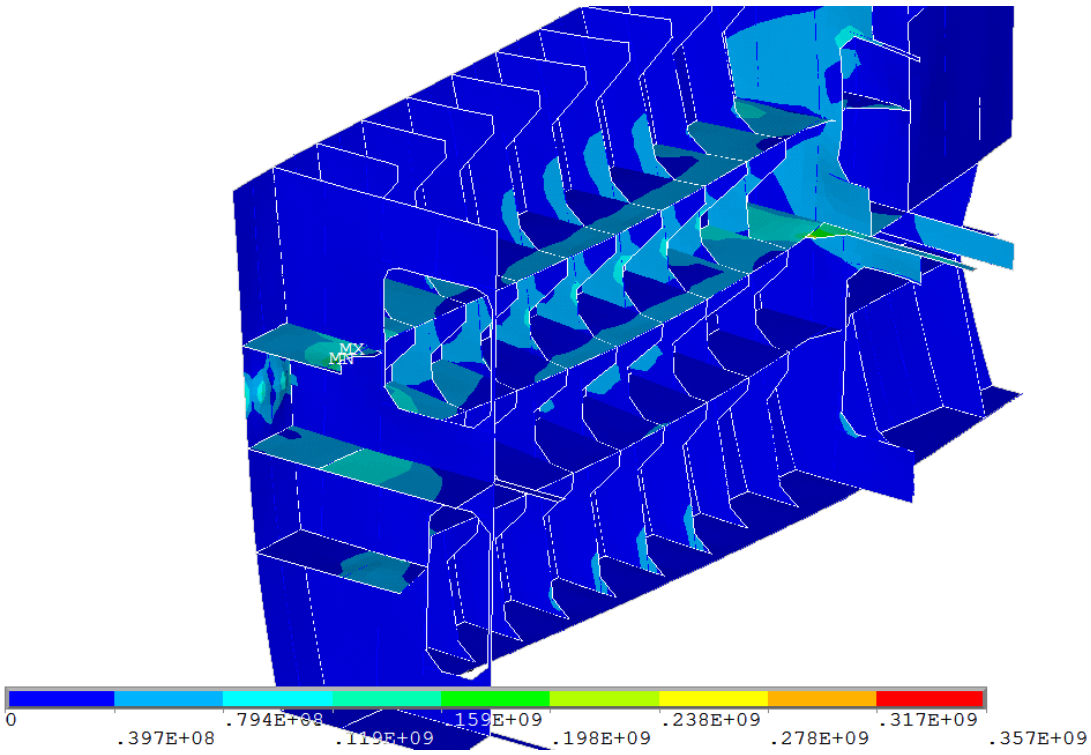

Figure 13: *von Mises stress* due to load case No. 3, ice belt region

Here it can be seen that higher stresses arise at the tapering of the web frames. The reason for this is that the structure of the frames becomes stiffer in the horizontal direction due to the "toe brackets"-like design. As expected, the stresses increase near the boundary conditions which were modeled as a rigid clamping, see Table 5. In the Figure 14 a zoom on the stress concentration can be seen. Through the structural idealization sharp edges were modeled and because of this modeling error high notch stresses can occur especially near the boundary conditions. In order to evaluate the stresses better the boundary effect should be cut off.

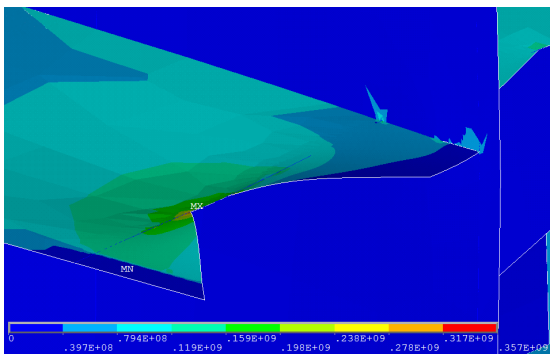

Figure 14: *von Mises stress* due to load case No. 3, zoom on stress concentration

In Figure 15 the same area is depicted but the boundary effect is cut off. Here it can be seen that near the bulkhead, which has a high stiffness, also high stresses occur.

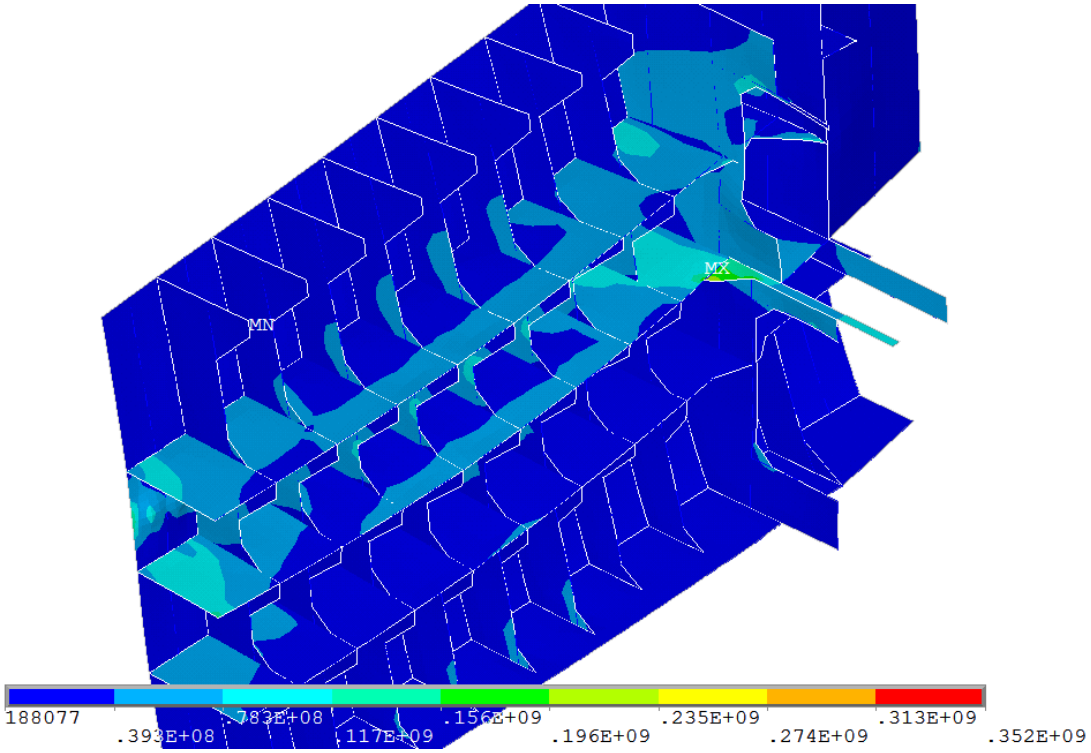

Figure 15: *von Mises stress* due to load case No. 3, ice belt region, cut off from boundary effects

Once again, through the structural idealization a sharp edge is modeled, which then results in a higher stress. The cut off of the deck at 7.30 m, where the stress concentration is located, is executed softer in reality. Beyond that nothing remarkable is to be observed.

Continuing with the load case No. 2, the *von Mises stress* of ice belt region is depicted in Figure 16. Again for visualization purposes, the section is rotated, so that the inner structure is visible. As in this load case the load is directly applied on the stringer, the stresses are less distributed over the shell but more over the supporting structures, i.e. the ice-stringer and the web frames.

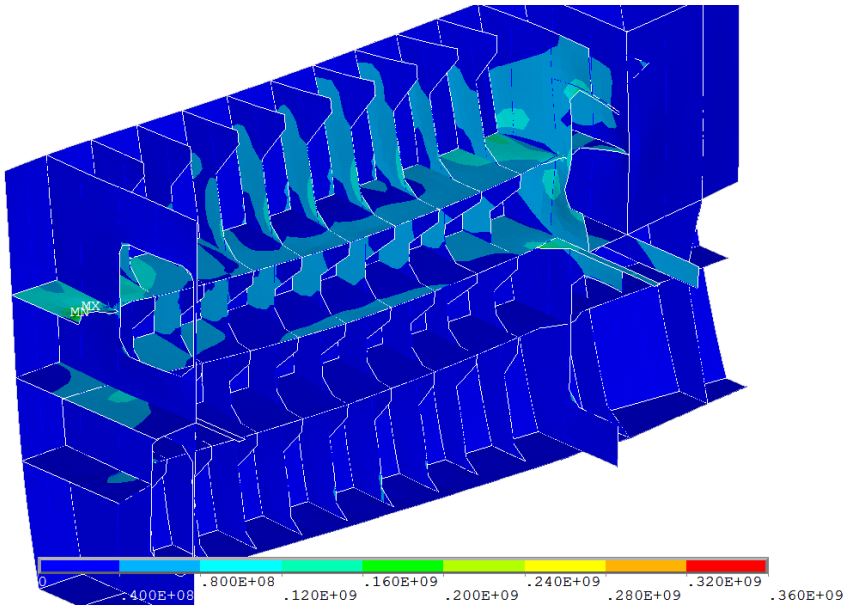

Figure 16: *von Mises stress* due to load case No. 2, ice belt region

Beyond that, nothing unusual can be observed that has not been discussed before.

9. Applicability of strain gauges for ice load measurement

In this section the theory of the applicability of strain gauges for ice load measurements will be pointed out. Besides, it will be shown how to implement this into a finite element analysis and last of all the possible sources of errors will be described. The following derivations are based upon [5].
The measurement approach with strain gauges is, that electrical resistors changing their resistance as they are lengthened. The advantage of strain gauges is that they convert the strain into an electrical signal. The mechanical quantity to be measured, the strain, produces a change in resistance in the strain gauge, which then changes the output voltage of the Wheatstone bridge circuit. The Wheatstone bridge circuit is a component of the strain gauge. In addition, the Wheatstone's bridge circuit offers an excellent possibility of largely compensating for the effects of undesirable influences such as those caused by temperature changes. For more detailed informations regarding the Wheatstone bridge the author refers to [11]. Further in text, the output voltage is then amplified and the thus produced measurement signal is displayed or recorded. The schema is shown in Figure 17.

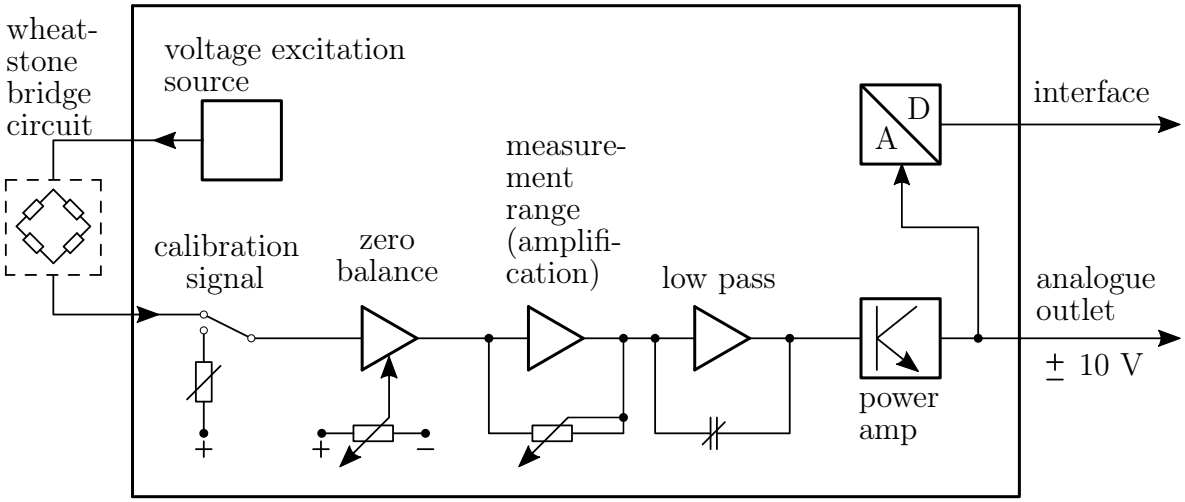

Figure 17: Concept of analogue measurement system with A/D-converter and digital output

9.1. Theory

In this subsection the theory of the applicability of strain gauges for ice load measurements on a ship's hull will be described, what possibilities of measurements are there, what needs to be considered and which approaches are used. Starting with the theory of the applicability of strain gauges for ice load measurements on a ship's hull. All insights are based on the bachelor thesis [22] and the dissertation [16]. Mainly there are two different approaches to measure ice-induced loads on a ship's hull. One is the indirect structural strain measurement and the other is the direct measurement of the contact pressure or load. In this thesis the indirect structural strain measurement will be used. In the indirect method, the strains are measured from the frame and the external loading is determined from the load-strain relation of the built structure which is determined by a finite element analysis. The shear strain-based measurements are sensitive to the location and length of the loading in the horizontal direction. Here is the assumption that the pressure distribution within the ice load patch acts uniform. In order to determine the force-strain relation of the structure an assumption about the location, shape, and pressure distribution has to be made. Commonly these are kept constant through the measurements but in reality they vary. One can imagine that the vertical location of the contact is affected by the draught and the movement of the ship [16]. For indirect strain gauge measurement of ice loads on a ship's hull mainly the two following strategies exist:

1. The measurement on the plate between the frames, this was conducted e.g by [9].

2. The measurement on frames with strain gauges at the end of the frame, close to the next higher supporting structure like [18] did it or distributed along the frame like [8] did it.

A combination of these strategies is possible as well. This thesis is focused on the second strategy with strain gauges at the end of the frame. Since the chosen set-up, measures the structural response, the structural ability to transfer loading should be understood. The load acts through the shell as a shear force on the frame. The reason for that is, as mentioned before, due to the ability of the structure to transport loading. One part of the loading is carried by the loaded frame and the other part is transported to the adjacent frames by the hull plating connecting the frames [16]. The amount of loading carried by the directly loaded frame depends on the topology of the frame structure. When the loading affects a frame directly, the shear force on the frame is a result of the deflection. The adjacent frame to the loaded frame undergoes deflection and rotation. The art's state of determining the load carried by the loaded frame is by using FEA [16]. Furthermore, the measurement frequency is important to differentiate between the sequential ice impacts. It is recommended to use a measurement frequency between 30 and 60 Hz. For an analysis of small subpeaks following each other a higher measurement frequency is needed, whereas for a slightly more imprecise result, the frequency can be reduced [22]. Moreover, the instrumented area has to be long enough in the vertical direction, since rolling and trimming of the ship during ice breaking and ramming, influence the area of the ice impacts.

9.2. Application

The calculation of the influence coefficient matrix $\boldsymbol{a}$ will be conducted on the section, between the deck 10.30 m above the Baseline and the ice-stringer 8.50 m above the Baseline. Since the second measurement strategy is chosen it is advantageous when there is a large distance between the supporting structure in vertical direction. Furthermore, this section lies in an area where the ship is usually operated. Due to the fact that the costs increase with the number of instrumenting frames, it is assumed that only five frames are instrumented. More precisely, the Frame 167 to Frame 171 will be instrumented. The shear strains are measured 0.3 m from the end of the frame, like [18] did it. In addition, the strain gauges should be located at the neutral axis because the shear strains and stresses obtain their maximum value at the neutral axis of the frame [16]. In Figure 18 a simplified cross section of a web frame is depicted. The assumption is that the cross section stays constant through the length of the web frame.

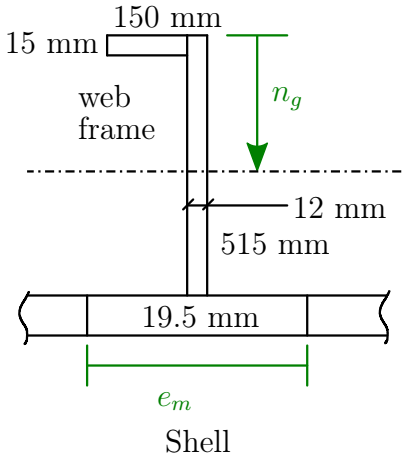

Figure 18: Cross section

In order to calculate the neutral axis of this cross section the effective width of the hull plating is determined using the *DNV GL* rules [1]. Two assumptions must be made in accordance with the regulations [1]. One assumption is that the girder is constrained on both ends and the other assumption is, that the girder is loaded by uniformly distributed loads or else by not less than 6 equally spaced single loads. According to this assumptions the length between zero-points reads as follows:

$$\ell = 0.6 \cdot 7400 \text{ mm} = 4440 \text{ mm} \tag{31}$$

Where 7400 mm is the distance between the bulkhead at Frame 164 and the bulkhead at Frame 174. The width of plating supporting is 370 mm. With the following ratio:

$$\frac{\ell}{e} = \frac{4440 \text{ mm}}{370 \text{ mm}} = 12 \tag{32}$$

The effective width of the hull plating reads $e_{m1} = 370$ mm. Thus the position of the neutral axis can be calculated. The neutral axis lies at $n_g = 345$ mm, which is also the center of gravity of this cross section in parallel direction to the frame.

For an overview, a short definition of the section to be instrumented is given and an illustration of an exemplary instrumentation of one frame is shown in Figure 19. The blue crosses show the position of the strain gauges.

- From the ice-stringer at 8.50 m above the Baseline
- To the deck 10.30 m above the Baseline
- Frame 167, Frame 168, Frame 169, Frame 170 and Frame 171

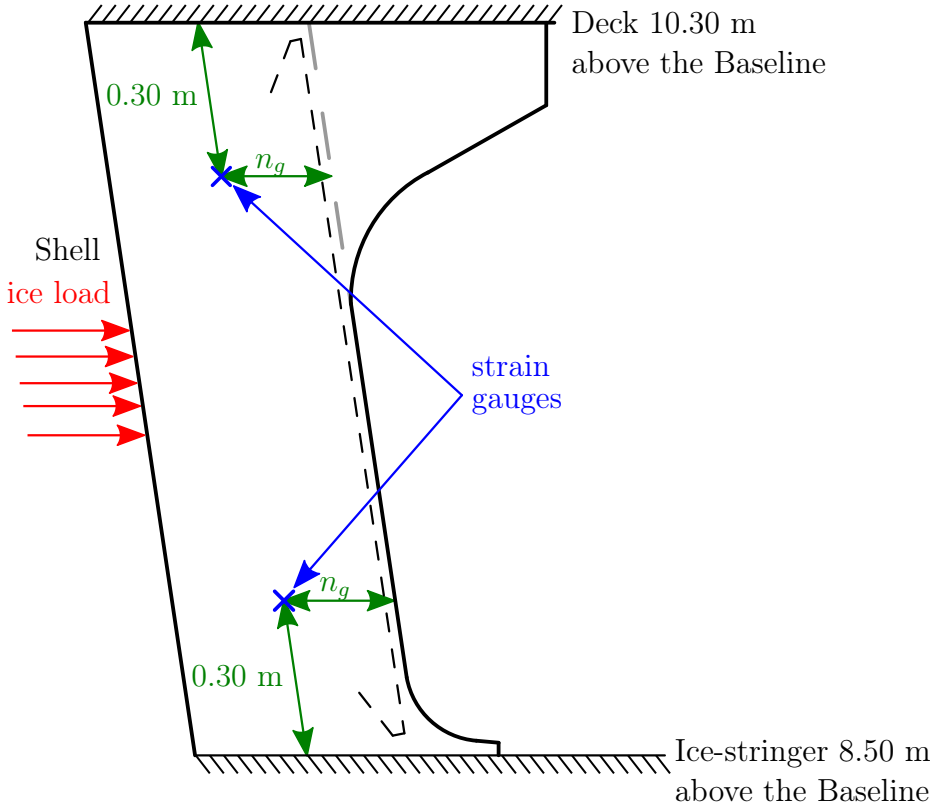

Figure 19: Exemplary instrumentation of the Frame 170

Thus, these are the positions on the frames where the shear strains are determined in the FEA.

9.3. Usage in FEM

In this subsection the usage of FEM will be described in order to calibrate the shear strain measurement system, so that future ice loads can be measured on the ships hull. All insights are based on [18] and [15]. The response of the adjacent frames can be accounted in the full-scale measurements by introducing an influence coefficient matrix. This concept assumes that a proportionality between the exerted force and the measured strains exists, where a proportionality factor is to be determined. One might say, that this proportionality factor behaves like the stiffness matrix $\boldsymbol{K}$. The assumption is then, so to say, that the structure behaves only elastic, which is not true in reality. Thus, the external load on the structure is determined from the measured shear strain difference with this influence coefficient matrix $\boldsymbol{a}$. The usage of the influence coefficient matrix can be seen in the following two equations:

$$\boldsymbol{F} = \boldsymbol{a}\Delta\boldsymbol{\gamma} \tag{33}$$

$$\boldsymbol{c}_{ij} = \Delta\boldsymbol{\gamma}_i \boldsymbol{F}_j \tag{34}$$

Where $\boldsymbol{a}$ is the influence coefficient matrix, $\boldsymbol{c}$ is the inverse matrix of $\boldsymbol{a}$, $\Delta\gamma_{i...m}$ is the shear strain difference measured on the frame i, m is the number of the instrumented frames and F_j is the external force exerted on the frame j. The diagonal terms of the influence coefficient matrix define the force-strain relation of the frame under loading and the off-diagonal terms determine the response of the adjacent frames. The difference in the shear strain between the ends of the frame, $\Delta\boldsymbol{\gamma}$, is determined by calculating the shear strain occurring at on the lower and upper parts of the frame with FEA and then calculating the difference. In order to determine the coefficients of the inverse influence coefficient matrix the unit load principle is used. This means that one frame at a time will be loaded by a force and the response of the frames, in terms of the shear strains, will be measured. The force should be high enough to take into account the influence on the adjacent frames, but it should also be possible to apply this force in reality by means of a calibration pull.
For the *HLL Rio de Janeiro* the influence coefficient matrix is calculated using FEA. The structural behavior was discussed in the Sections 8 and so the calculation will be conducted on the same FEM-model as in this section. In order to calculate the influence coefficient matrix a unit load of 10 kN is chosen. This load will be applied in the middle of the frame. The shear strains will be measured on the same places like it is depicted in the Figure 19. Conducting this procedure leads to the following influence coefficient matrix.

$$\boldsymbol{a} = \begin{bmatrix} 4.7410 & -0.0882 & -0.0172 & -0.0127 & -0.0076 \\ -0.0674 & 4.4278 & -0.0758 & -0.0175 & -0.0099 \\ -0.0429 & -0.0993 & 5.0792 & -0.0763 & -0.0158 \\ -0.0260 & -0.0364 & -0.0561 & 4.2753 & -0.0653 \\ -0.0193 & -0.0240 & -0.0299 & -0.0464 & 4.1850 \end{bmatrix} \cdot 10^5 \text{ [kN]} \tag{35}$$

9.4. Possible sources of errors

In this subsection the possible sources of errors within the measurement set-up will be described in order to evaluate the future outcomes out of the ice load measurement properly. First of all, it is important to know, when the location of the loading is not between the sensors, in vertical direction, the measurement fails as the method does not account for the loading having an effect outside the measurement area. A similar problem occurs in the horizontal direction. The measurements only account for the location of the instrumentation, since the loads are measured of a local structure and so no knowledge about the surrounding, not instrumented, structure is obtained. But, one can imagine, that a loading outside the measurement area can affect the measurements since the loading is transferred between the frames through the plates. An other problem is, that the *HHL Rio de Janeiro* has the second highest ice class which implies, that the structure in the ice belt region is rather stiff. Thus, the response to smaller loads is minimal and difficult to measure, as the strain gauges are commonly optimize for higher loads [16]. As a consequence, it can be impossible to separate the smaller loads form the noise of the carrier voltage of the measurement system. In addition, the pressure distribution within the contact area in the horizontal direction and the load length are the main uncertainties affecting the measurement results in shear strain difference-based measurements [16].
To be mentioned is, that the maintenance of such a shear strain measurement set-up for ice load measurement on a ship's hull requires higher personnel needs. Ideally, the installation of this measurement set-up should be as easy as possible, yet the working environment in ships is challenging for strain gauge measurements. The main problems of the measurement set-up is the location of the power supply and the attachment of the cables, which can be long, depending on the environment. In addition physical problems occur like humidity, cold temperatures, high velocity's, accelerations and vibration. These problems affect not only the measuring system but also the personnel. What's more is the possibility of confined space, low sources of light, air ventilation and limited possibilities for the transportation of the measurement devices.

10. Conclusion

The shipowner is interested in instrumenting one of his ships for ice load measurements in order to get a better knowledge about the ice-structure interaction on the ship's hull. In this case it concerns the ship *HLL Rio de Janeiro*. A suitable measurement method has been selected for this purpose. The measurement uses strain gauges as the main component. Besides, the method used is the measurement of shear strains on the frame with strain gauges at the end of each instrumented frame near the next higher supporting structure, see Figure 19. In order to consider the relation between measured shear strains and the ice load correctly, an influence coefficient matrix is calculated using FEM. The assumptions and limitations of the used measuring system are described in Chapter 9. Mainly, the pressure distribution within the contact area in the horizontal direction and the load length are the main uncertainties affecting the measurement results in shear strain difference-based measurements [16].
A rather large area of the ship was modeled as a 2D surface model. For modeling, the the grommet store was chosen. This room is best suited for the measurements because it has good access to electricity and an overall good accessibility. In retrospect, the author recommends to do the modeling completely in a CAE program of your choice as long as it is possible. Thus import problems can be avoided. In this case, the modeling should have been performed completely in *ANSYS 18.2*. With structural idealization, one should rather accept a high aspect ratio, which increases the calculation time, and model the cut-outs as constructed. This makes the solution generally more accurate and easier to evaluate, since modeling errors can be better distinguished from singularities. In further work, the influence of the boundary conditions on the solution could be examined more closely. In this case, a fixed clamping was assumed as a boundary condition. Before the influence coefficient matrix was calculated, a general analysis of the structure was conducted. Here the design loads from the FSICR [19] from 2008 were applied. The detailed description of the results can be found in Chapter 8.
It is assumed that the analysis provided realistic results. In order to verify the results, a mesh convergence study should have been conducted. The general steps for a mesh convergence study are the following. First a mesh is created using the lowest reasonable number of elements with the subsequent analysis of the model. Then the mesh is recreated with a denser element distribution, then re-analyzed and then the results will be compared with those of the previous mesh. The mesh density will be increased until the results converge satisfactorily.
The calculation of the influence coefficient matrix followed. The result can be seen in the following Equation.

$$\boldsymbol{a} = \begin{bmatrix} 4.7410 & -0.0882 & -0.0172 & -0.0127 & -0.0076 \\ -0.0674 & 4.4278 & -0.0758 & -0.0175 & -0.0099 \\ -0.0429 & -0.0993 & 5.0792 & -0.0763 & -0.0158 \\ -0.0260 & -0.0364 & -0.0561 & 4.2753 & -0.0653 \\ -0.0193 & -0.0240 & -0.0299 & -0.0464 & 4.1850 \end{bmatrix} \cdot 10^5 \text{ [kN]} \tag{36}$$

The comparison with the matrix of [18] shows similar results. Nevertheless, the correctness of this matrix should be determined by a calibration test.

References

[1] DNV GL. *Rules for classification; Part 3 Structures, equipment; Chapter 3 Hull girder strength*. DNV GL, 2015.

[2] A. Düster. *High-Order FEM - Lecture Notes*. Technische Universität Hamburg, 2010.

[3] A. Düster. *Structural Analysis of Ships and Offshore Structures - Lecture Notes*. Technische Universität Hamburg, 2015.

[4] A. Haque. *Introduction to Timoshenko Beam Theory*. Elsevier, 2016.

[5] S. Keil. *Dehnungsmessstreifen*. Springer Fachmedien Wiesbaden, Wiesbaden, 2nd ed. edition, 2017.

[6] P. Kujala. *Results of long-term ice load measurements on board chemical tanker M/S Kemira in the Baltic sea during the winters 1985 to 1988*. POAC 1989, Proceedings Vol. 2, Luleå, 12-16 June: 1118-1129, 1989.

[7] P. Kujala, M. Suominen, and K. Riska. *Statistics of ice loads measured on MT Uikku in the Baltic*. POAC 2009, Proceedings, Luulaja, 9-12 June, 2009.

[8] L. Müller and H. G. Payer. Loads on research vessel polarstern under arctic conditions. *Port and Ocean engineering under Arctic Conditions 1987*, 1:495–508, 1988.

[9] T.-K. Lee, J.-H. Lee, H. Kim, and C. W. Rim. Field measurement of local ice pressures on the araon in the beaufort sea. *International Journal of Naval Architecture and Ocean Engineering*, 6(4):788–799, 2014.

[10] J.-R. Sack and J. Urrutia, editors. *Handbook of computational geometry*. Elsevier, Amsterdam, 1st ed. edition, 2000.

[11] C. A. Sciammarella and F. M. Sciammarella. *Experimental mechanics of solids*. John Wiley & Sons, Hoboken, NJ, 2012.

[12] sharcnet.ca. 4.4.1. understanding the plasticity models. `https://www.sharcnet.ca/Software/Ansys/17.0/en-us/help/ans_mat/amp8sq21dldm.html`. Date accessed: 24.09.2018.

[13] sharcnet.ca. Beam188 3-d linear finite strain beam. `https://www.sharcnet.ca/Software/Ansys/17.0/en-us/help/ans_elem/Hlp_E_BEAM188.html`. Date accessed: 24.09.2018.

[14] sharcnet.ca. Shell181 4-node structural shell. `https://www.sharcnet.ca/Software/Ansys/16.2.3/en-us/help/ans_elem/Hlp_E_SHELL181.html`. Date accessed: 24.09.2018.

[15] C. G. Soares and R. A. Shenoi, editors. *Analysis and design of marine structures V: Proceedings of the 5th International Conference on Marine Structures (MARSTRUCT 2015), Southampton, UK, 25-27 March 2015*. CRC Press/Balkema, Leiden, The Netherlands, 2015.

[16] M. Suominen. *Uncertainty and variation in measured ice-induced loads on a ship hull*. Department of Mechanical Engineering, Aalto University, 2018.

[17] M. Suominen, J. Karhunen, A. Bekker, P. Kujala, M. Elo, von Bock und Polach, Rüdiger, H. Enlund, and S. Saarinen. *Full-scale measurements on board PSRV S.A. Agulhas II in the Baltic sea*. POAC 2013, Proceedings, Espoo, 9-13 June, 2013.

[18] M. Suominen, P. Kujala, J. Romanoff, and H. Remes. Influence of load length on short-term ice load statistics in full-scale. *Marine Structures*, 52:153–172, 2017.

[19] Swedish Maritime Administration. *Finnish-Swedish ice class rules 2008*. Swedish Maritime Administration, Helsinki, 08.12.2008.

[20] wikipedia.org. Von mises yield criterion. `https://en.wikipedia.org/wiki/Von_Mises_yield_criterion`. Date accessed: 24.09.2018.

[21] P. Wriggers. *Nonlinear Finite Element Methods*. Springer Berlin Heidelberg, Berlin, Heidelberg, 2008.

[22] T. Zorn. *Strain-gauge-based measurements of ice loads on ships*. Institute for Ship Structural Design and Analysis, Hamburg University of Technology, 2018.

A. Appendix

A.1. Evaluation of load case No. 1

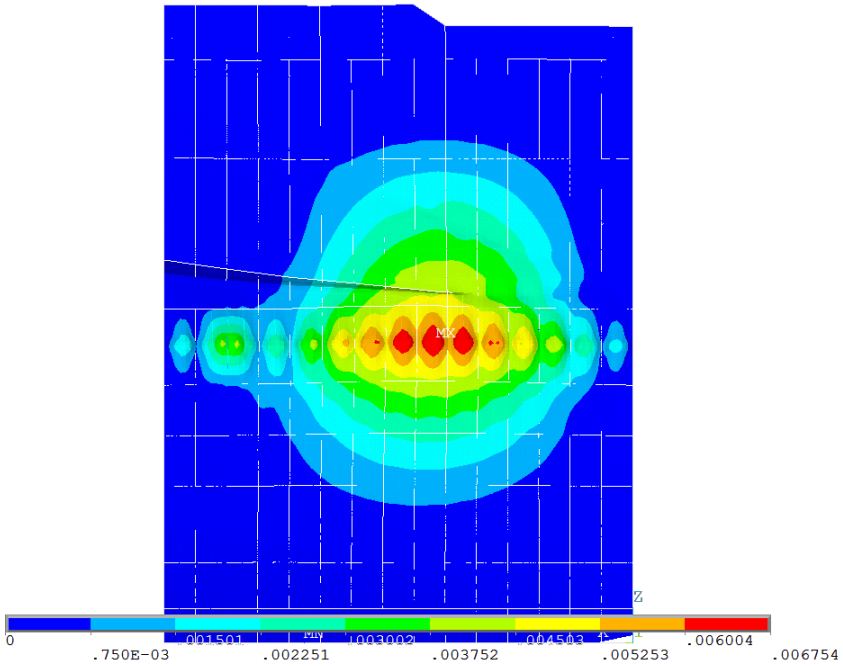

Figure 20: Displacement due to load case No. 1

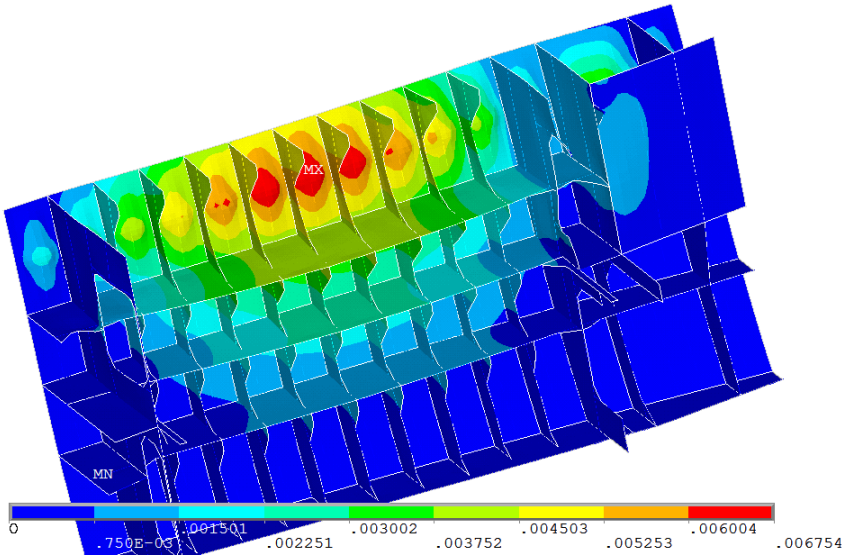

Figure 21: Displacement due to load case No. 1, ice belt region

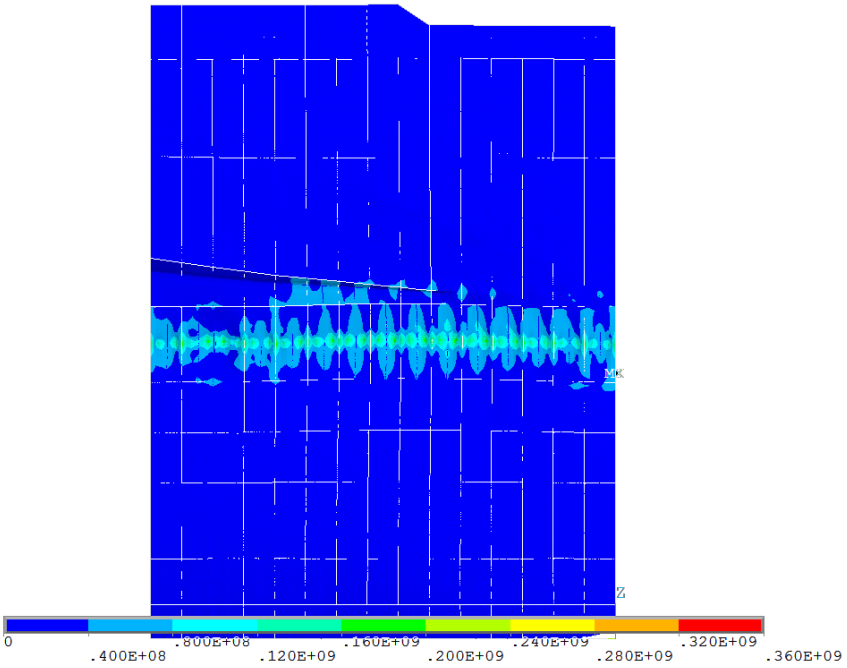

Figure 22: *von Mises stress* due to load case No. 1

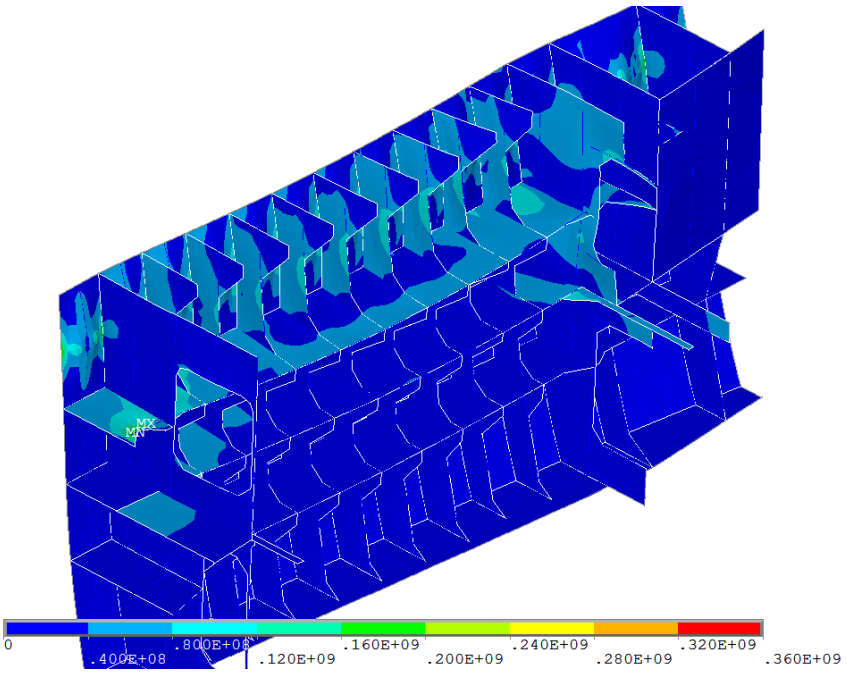

Figure 23: *von Mises stress* due to load case No. 1, ice belt region

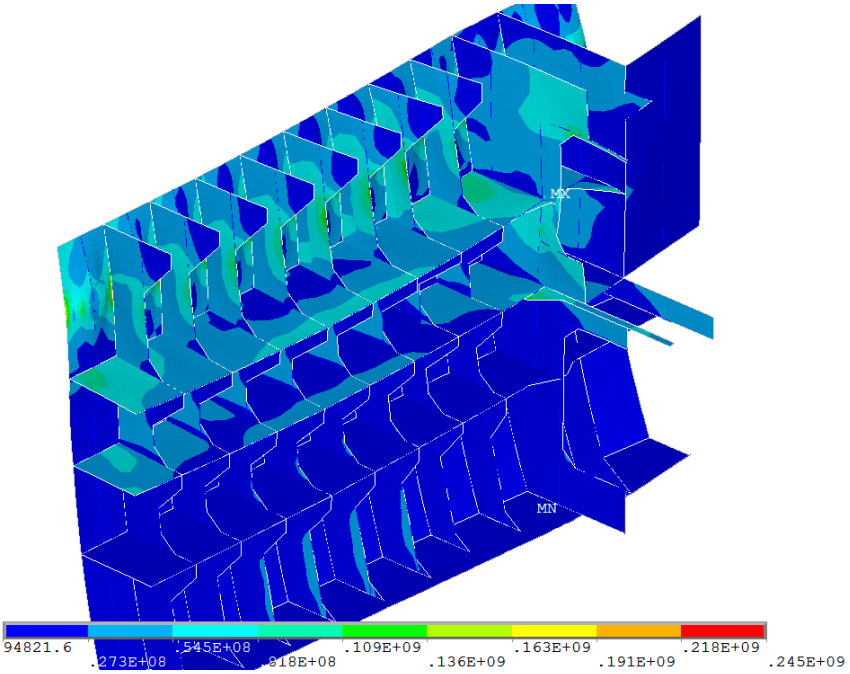

Figure 24: *von Mises stress* due to load case No. 1, ice belt region, cut off from boundary effects

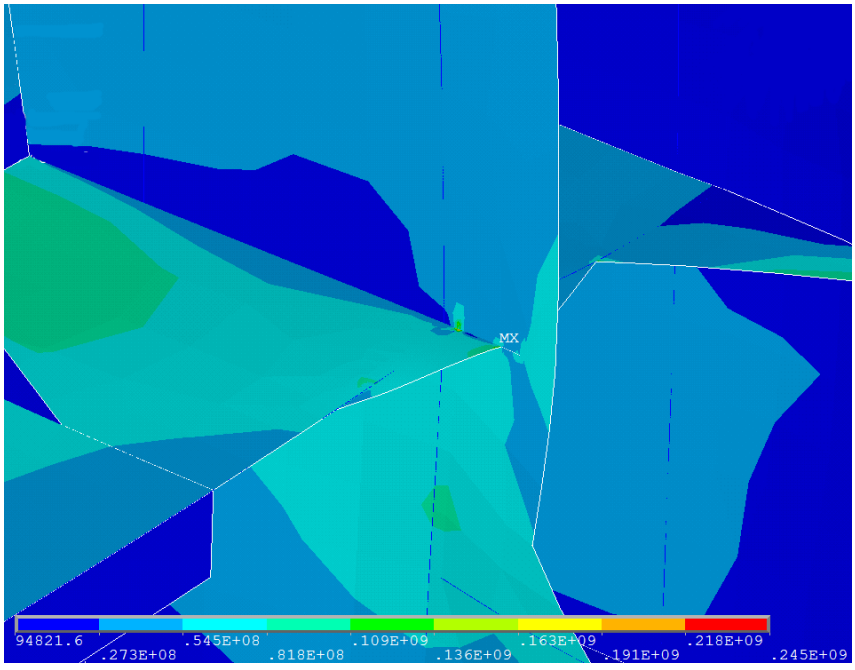

Figure 25: *von Mises stress* due to load case No. 1, cut off from boundary effects, zoom on stress concentration

A.2. Evaluation of load case No. 2

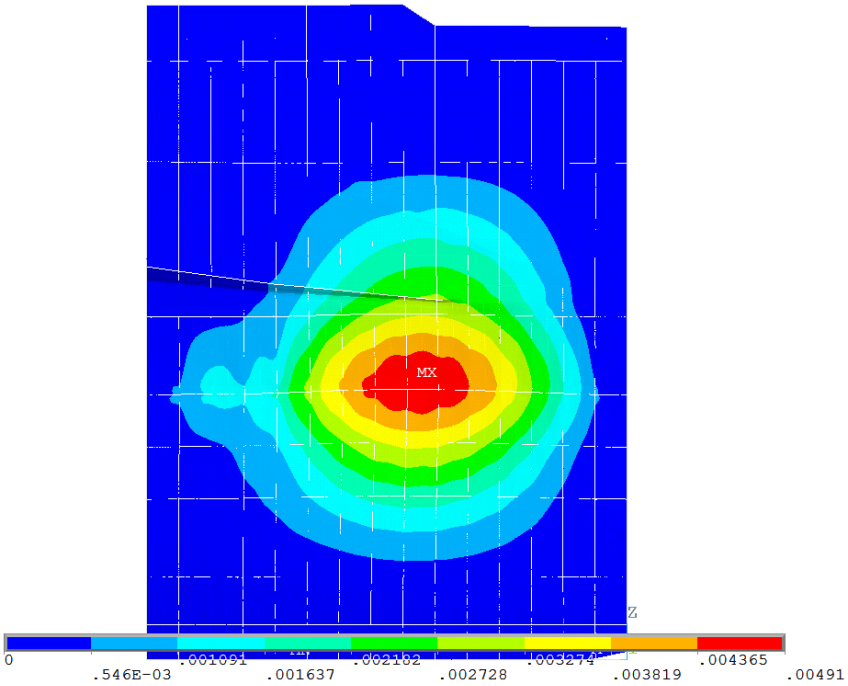

Figure 26: Displacement due to load case No. 2

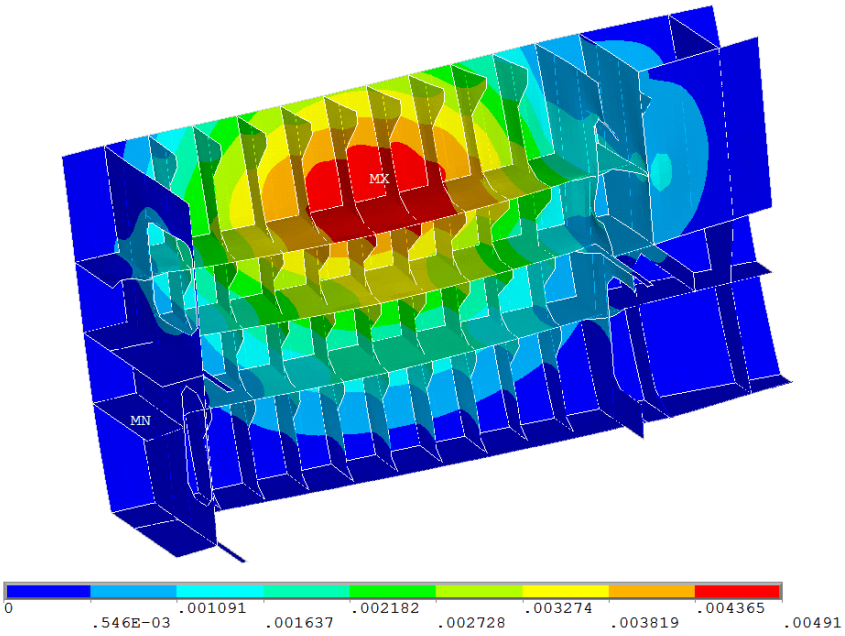

Figure 27: Displacement due to load case No. 2, ice belt region

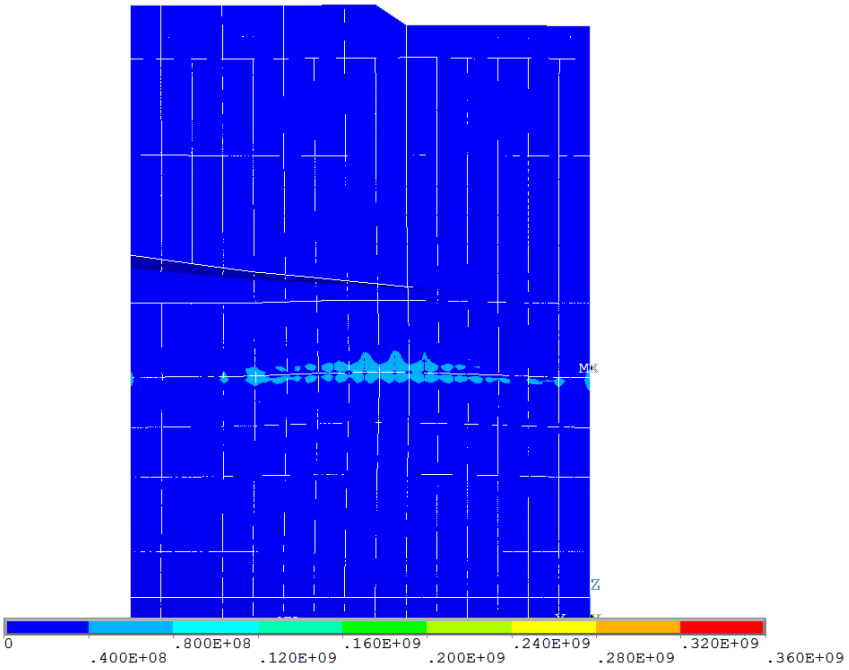

Figure 28: *von Mises stress* due to load case No. 2

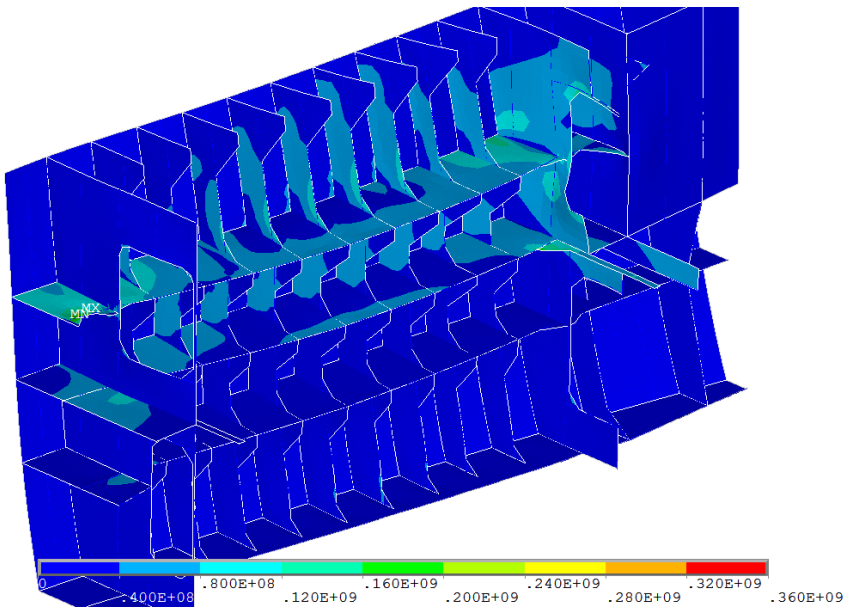

Figure 29: *von Mises stress* due to load case No. 2, ice belt region

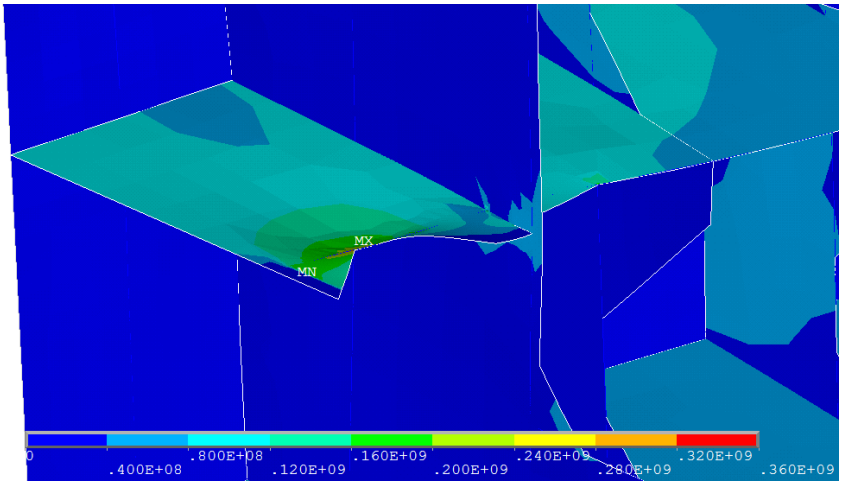

Figure 30: *von Mises stress* due to load case No. 2, zoom on stress concentration

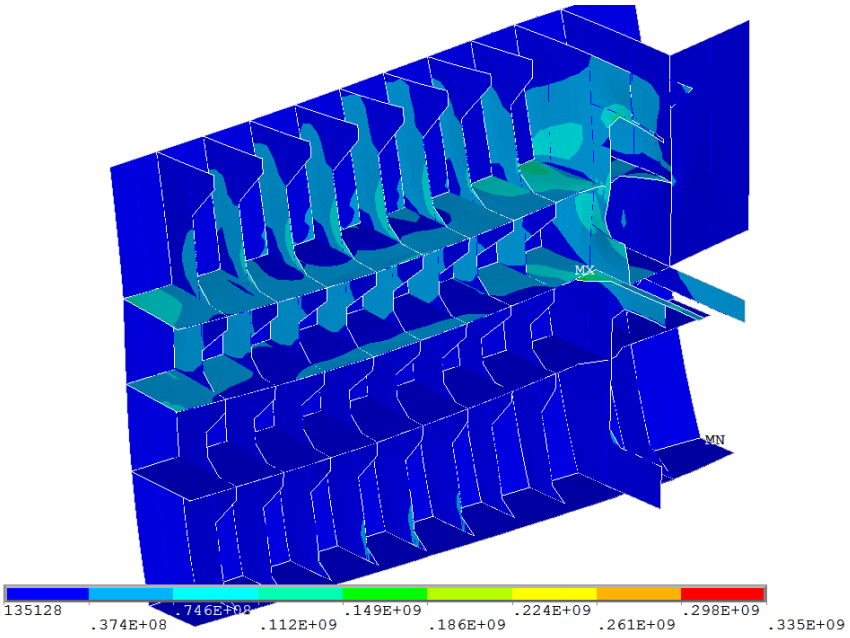

Figure 31: *von Mises stress* due to load case No. 2, ice belt region, cut off from boundary effects

A.3. Evaluation of load case No. 3

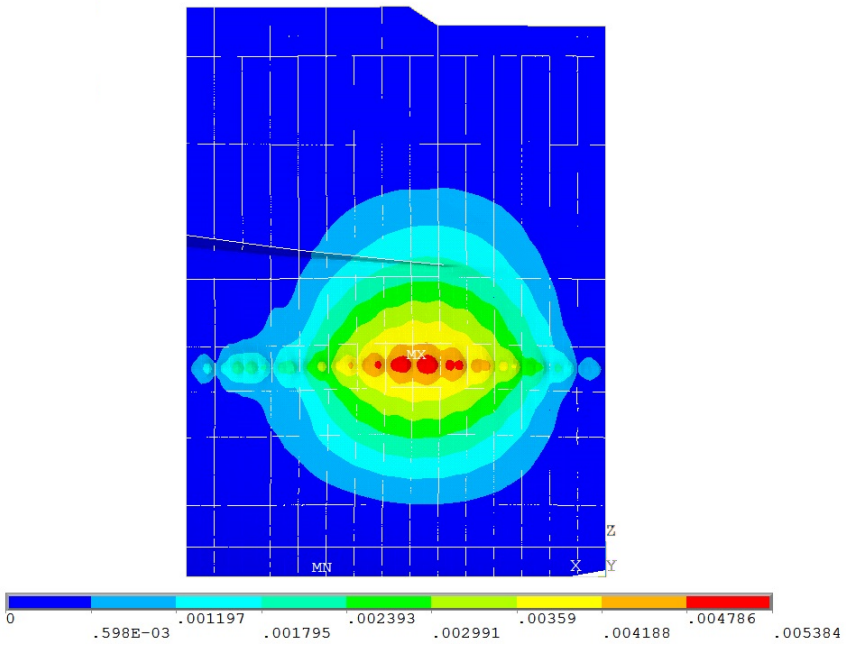

Figure 32: Displacement due to load case No. 3

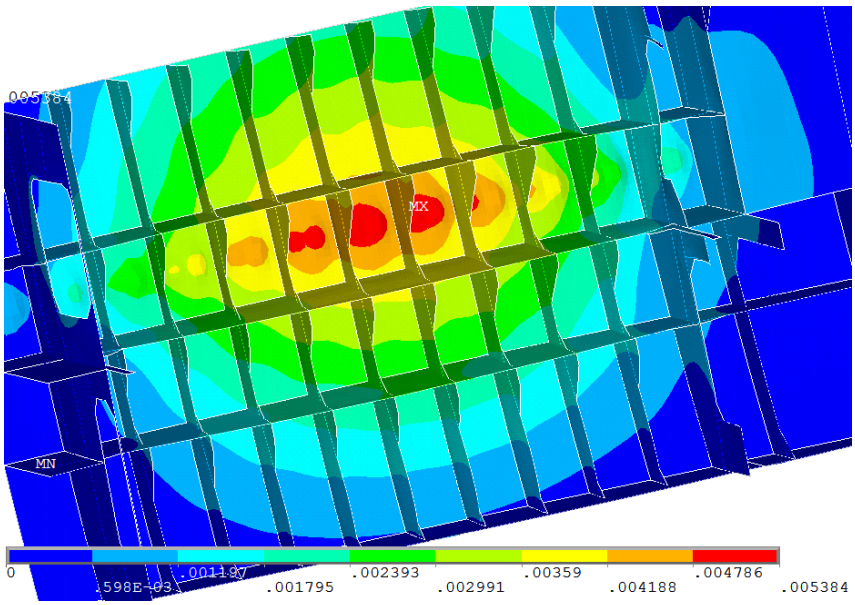

Figure 33: Displacement due to load case No. 3, ice belt region

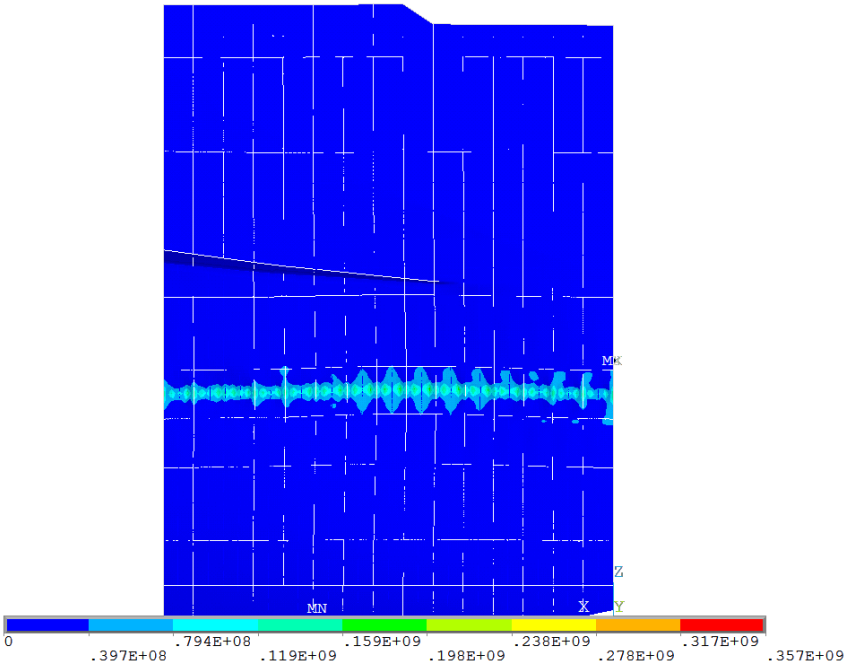

Figure 34: *von Mises stress* due to load case No. 3

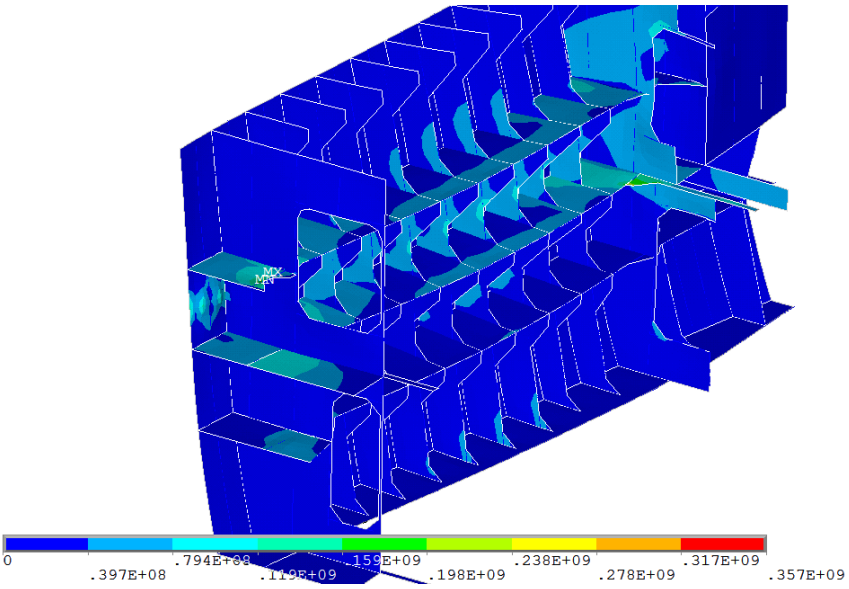

Figure 35: *von Mises stress* due to load case No. 3, ice belt region

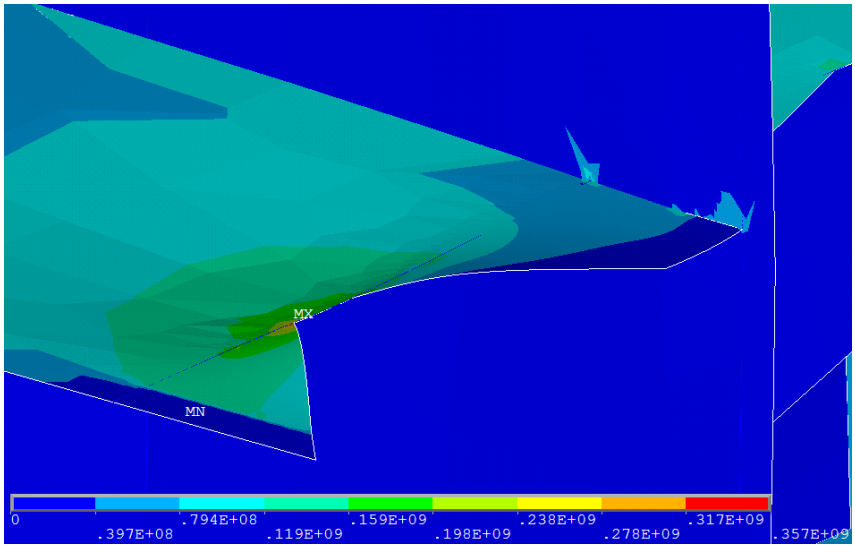

Figure 36: *von Mises stress* due to load case No. 3, zoom on stress concentration

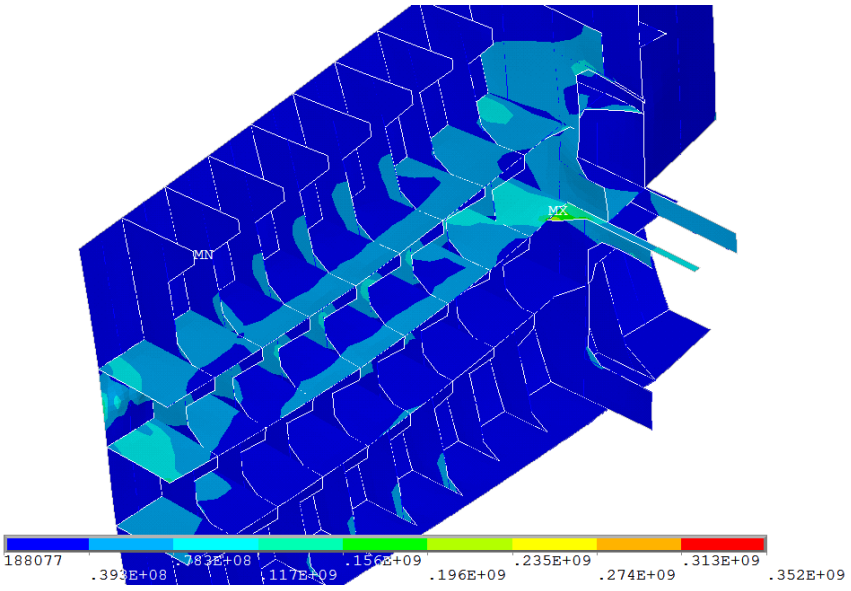

Figure 37: *von Mises stress* due to load case No. 3, ice belt region, cut off from boundary effects

A.4. Evaluation of load case No. 4

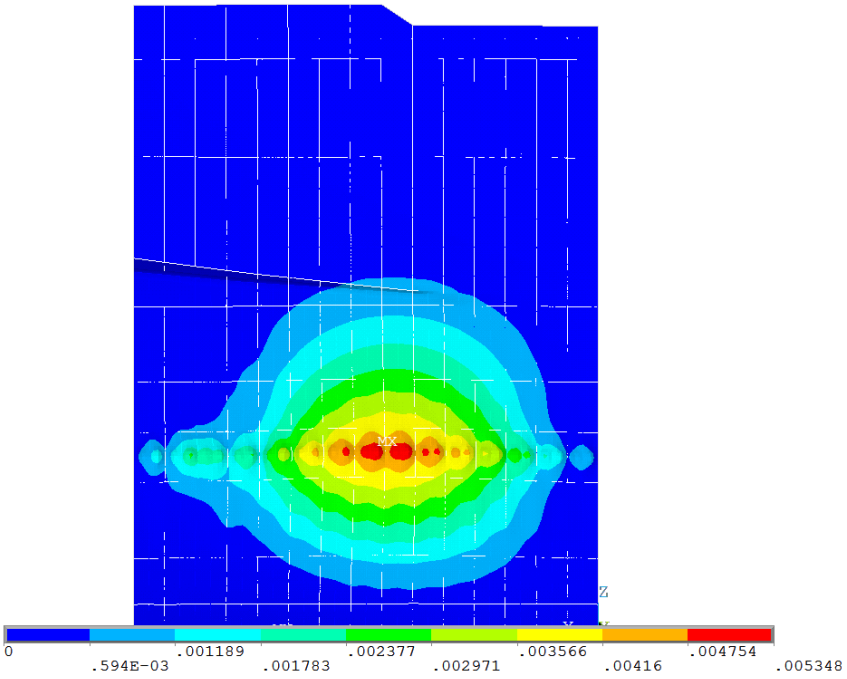

Figure 38: Displacement due to load case No. 4

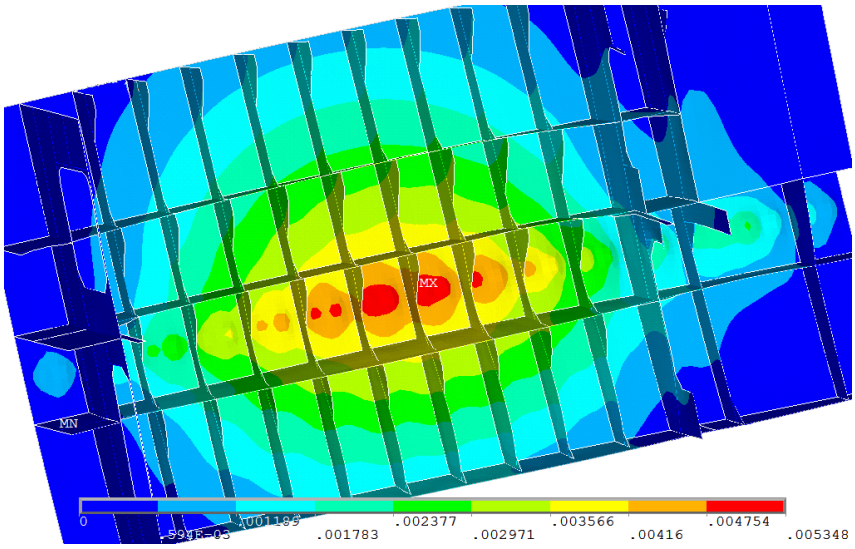

Figure 39: Displacement due to load case No. 4, ice belt region

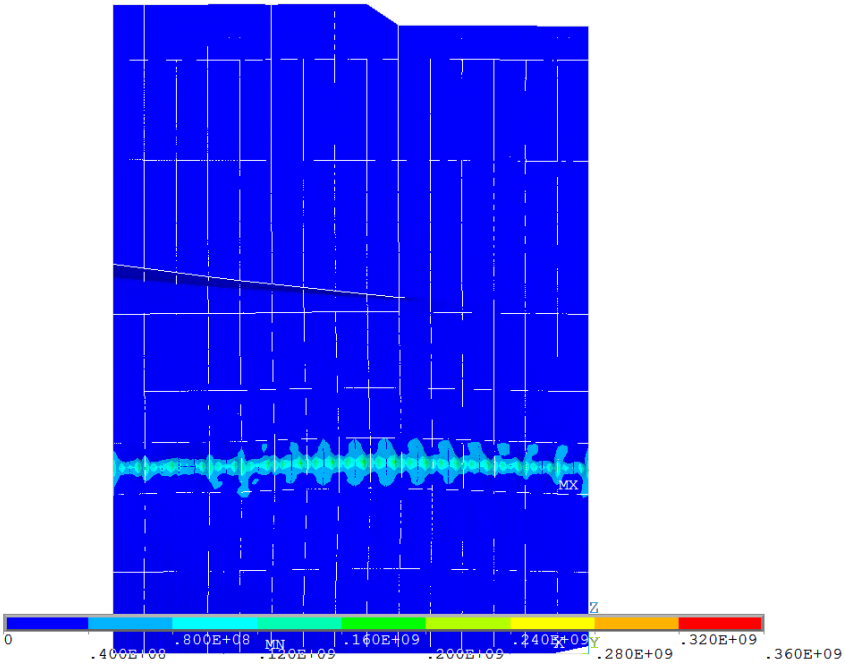

Figure 40: *von Mises stress* due to load case No. 4

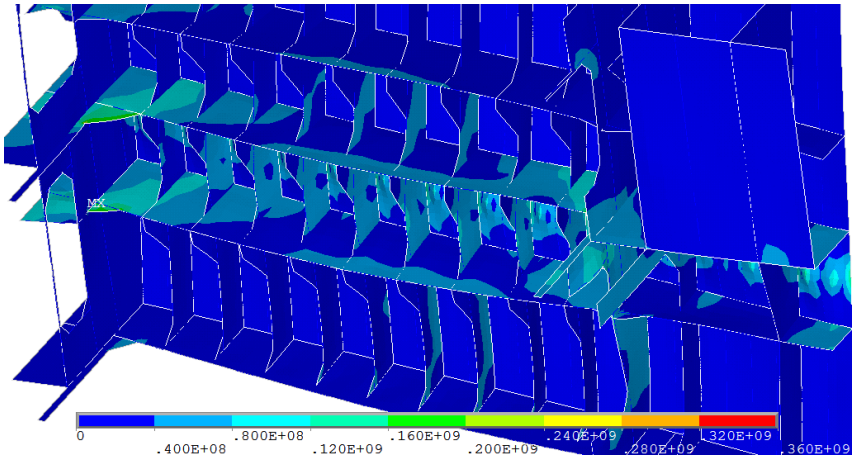

Figure 41: *von Mises stress* due to load case No. 4, ice belt region

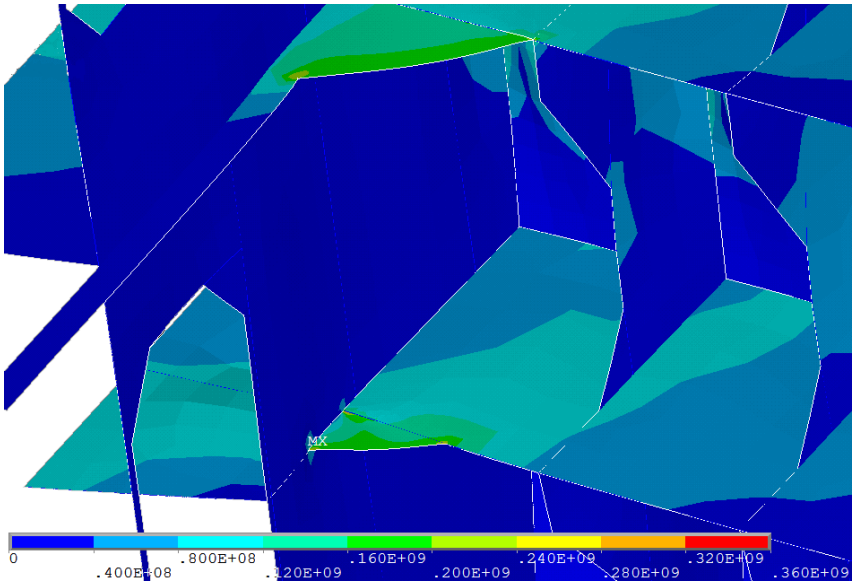

Figure 42: *von Mises stress* due to load case No. 4, zoom on stress concentration

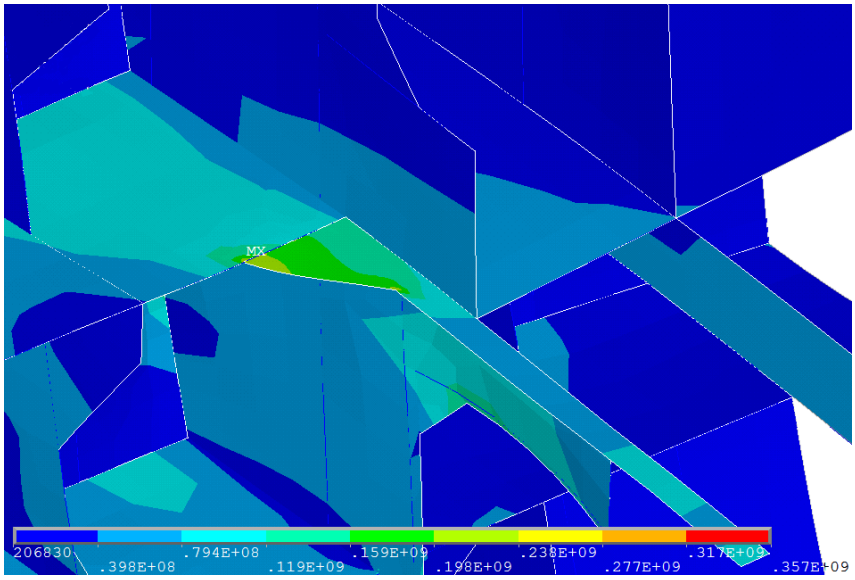

Figure 43: *von Mises stress* due to load case No. 4, ice belt region, cut off from boundary effects, zoom on stress concentration

A.5. Evaluation of load case No. 5

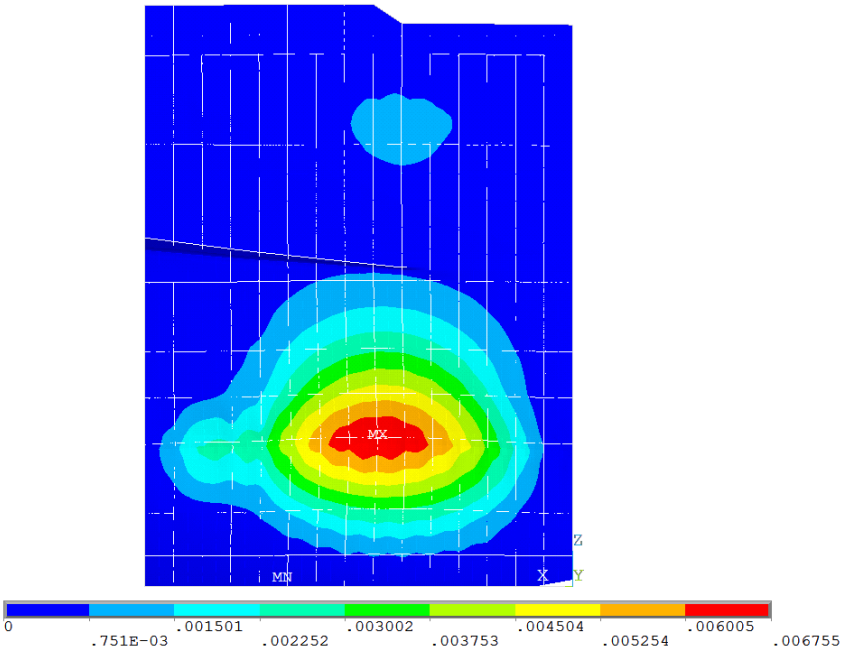

Figure 44: Displacement due to load case No. 5

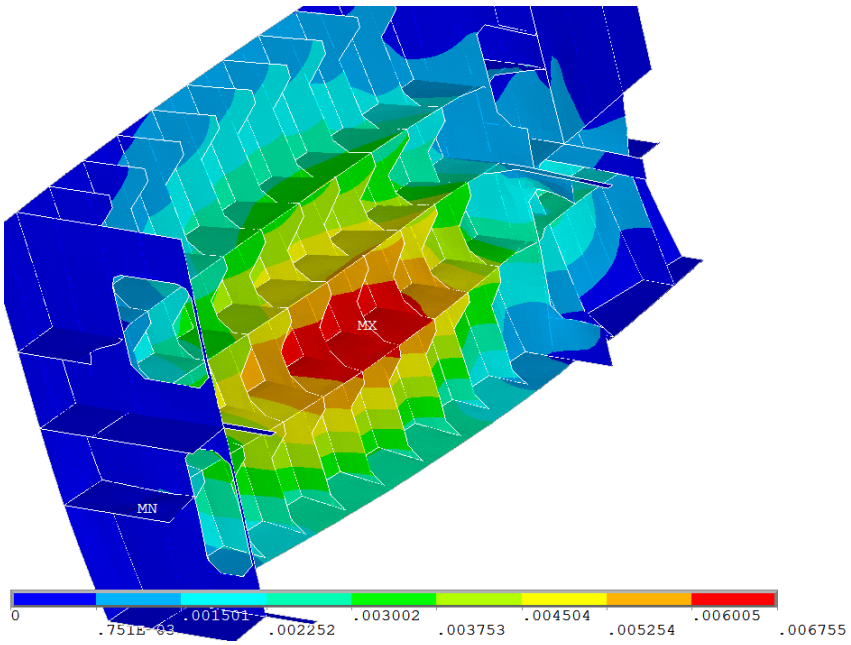

Figure 45: Displacement due to load case No. 5, ice belt region

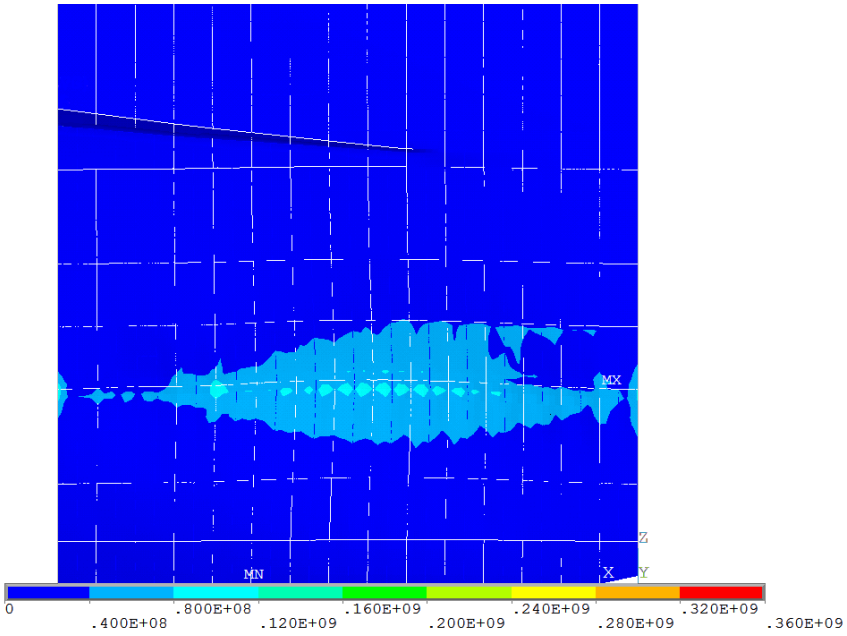

Figure 46: *von Mises stress* due to load case No. 5

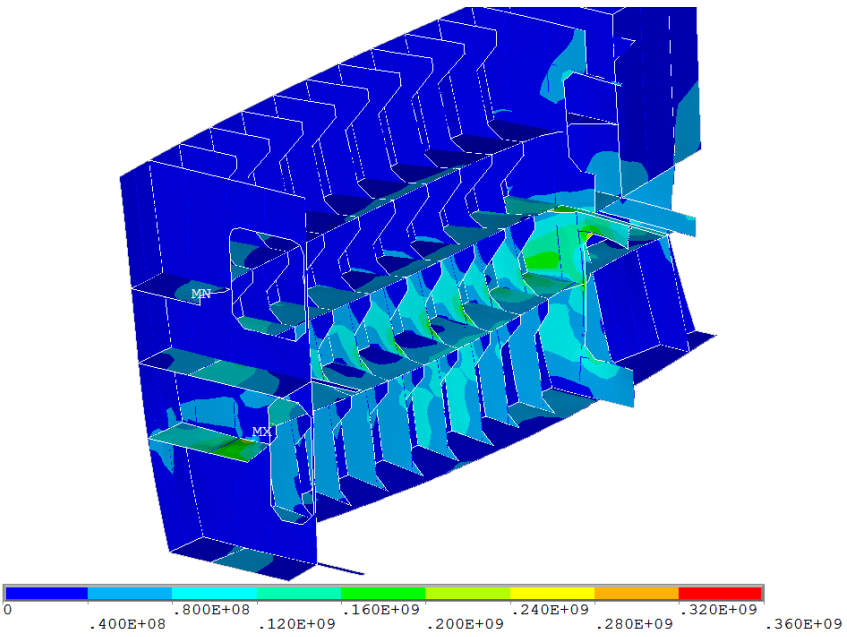

Figure 47: *von Mises stress* due to load case No. 5, ice belt region

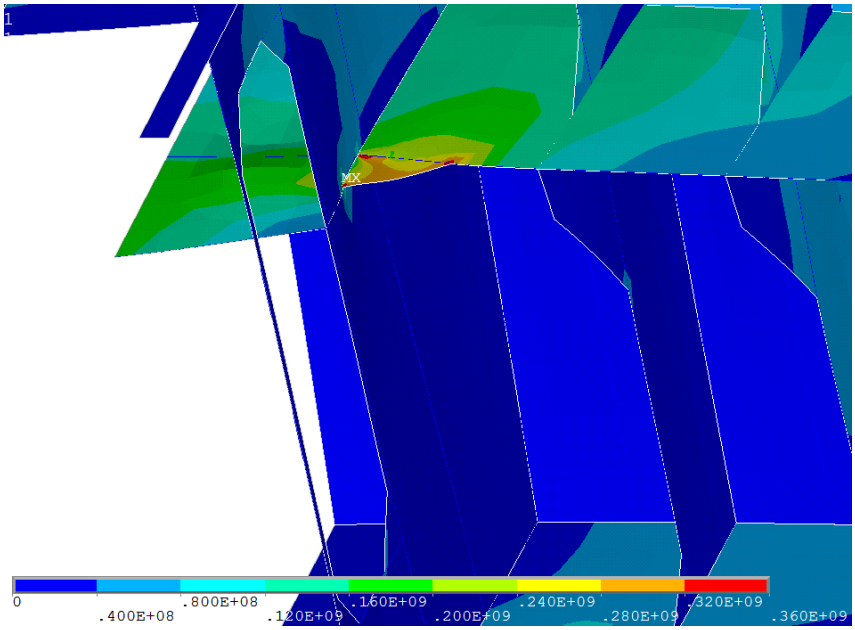

Figure 48: *von Mises stress* due to load case No. 5, ice belt region, zoom on stress concentration

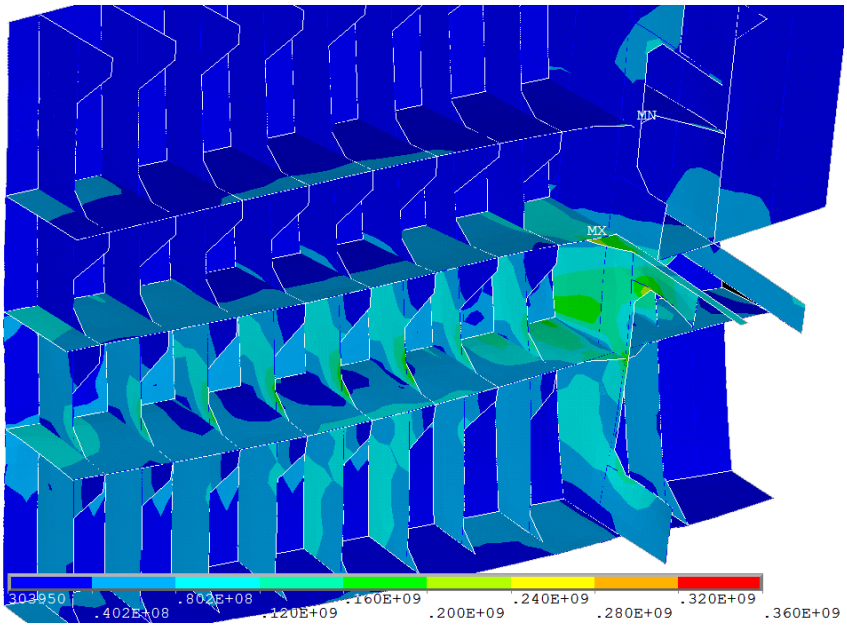

Figure 49: *von Mises stress* due to load case No. 5, cut off from boundary effects

A.6. Evaluation of load case No. 6

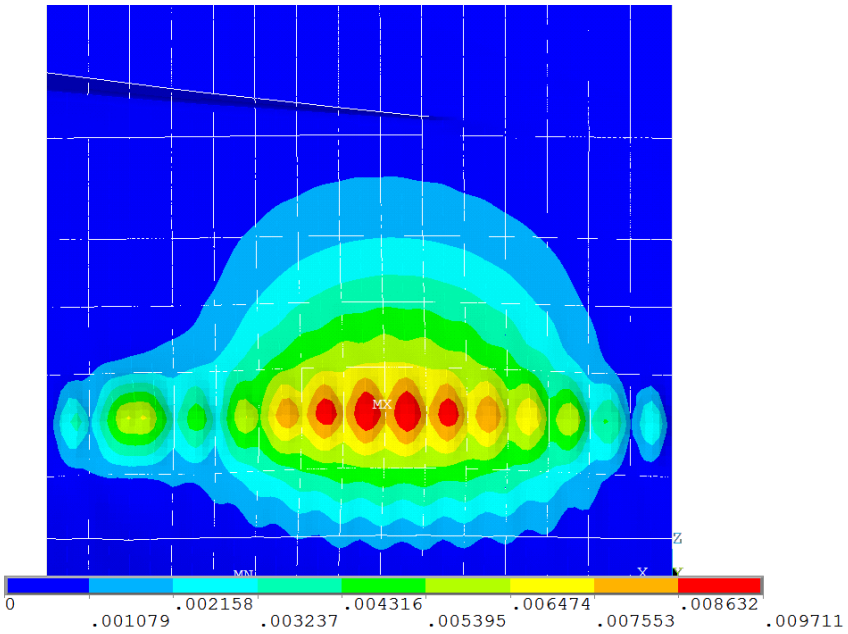

Figure 50: Displacement due to load case No. 6

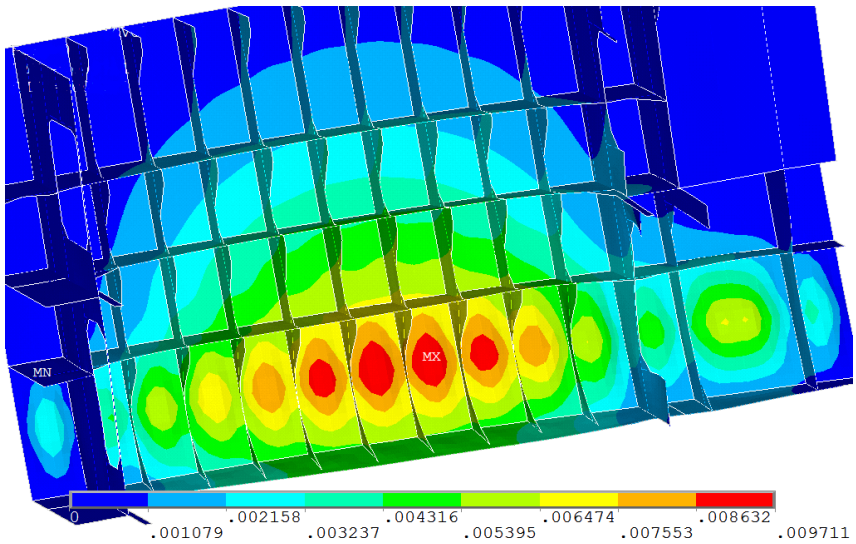

Figure 51: Displacement due to load case No. 6, ice belt region

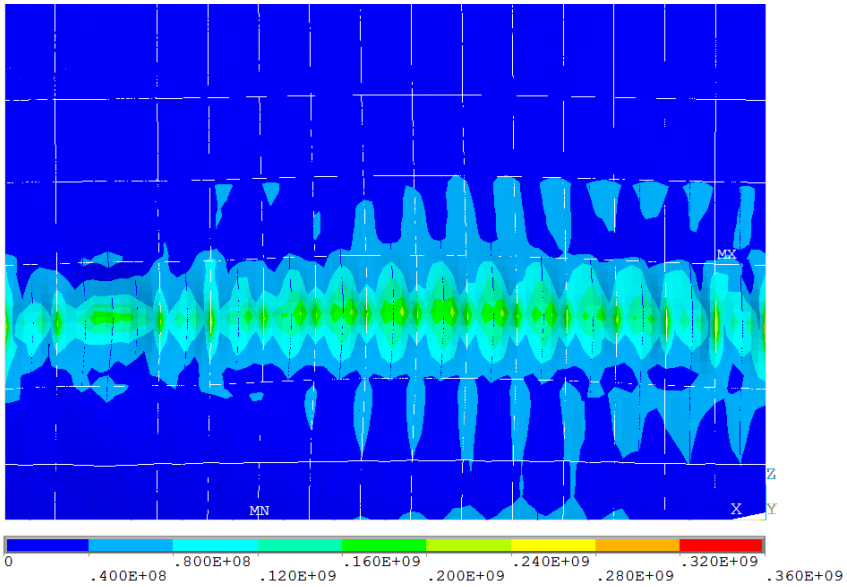

Figure 52: *von Mises stress* due to load case No. 6

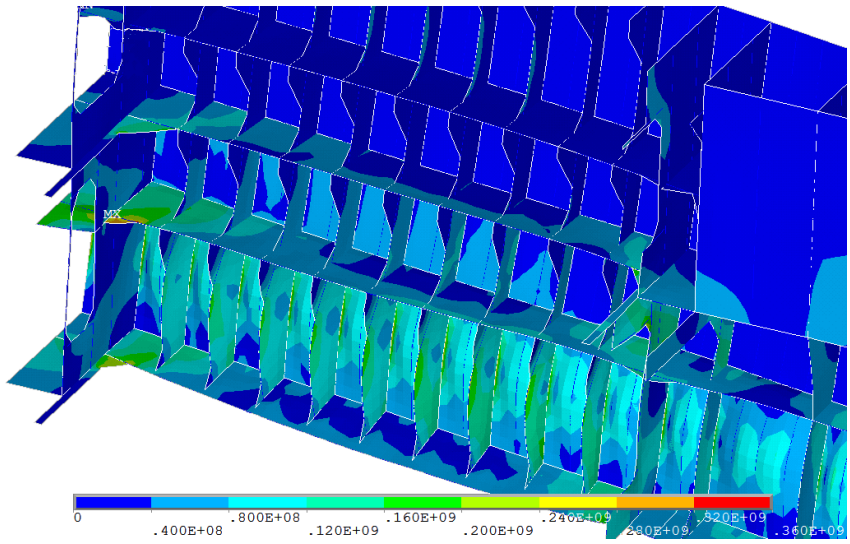

Figure 53: *von Mises stress* due to load case No. 6, ice belt region

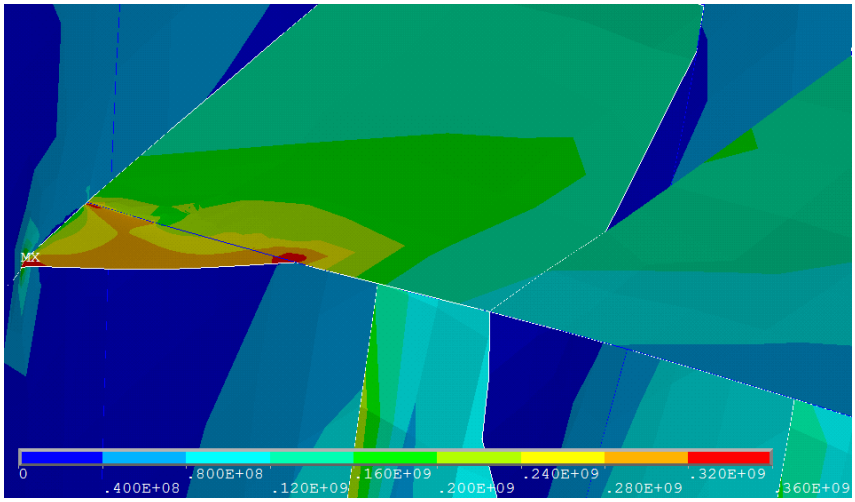

Figure 54: *von Mises stress* due to load case No. 6, zoom on stress concentration

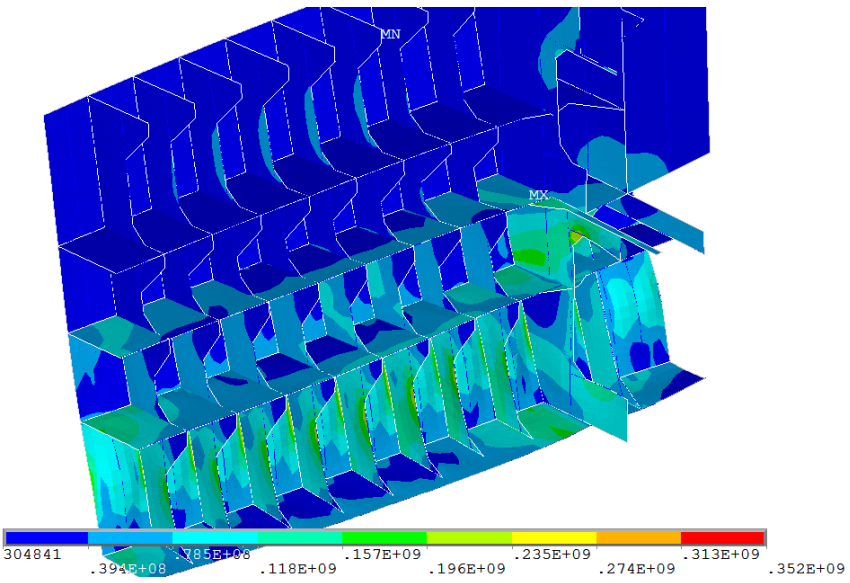

Figure 55: *von Mises stress* due to load case No. 6, ice belt region, cut off from boundary effects

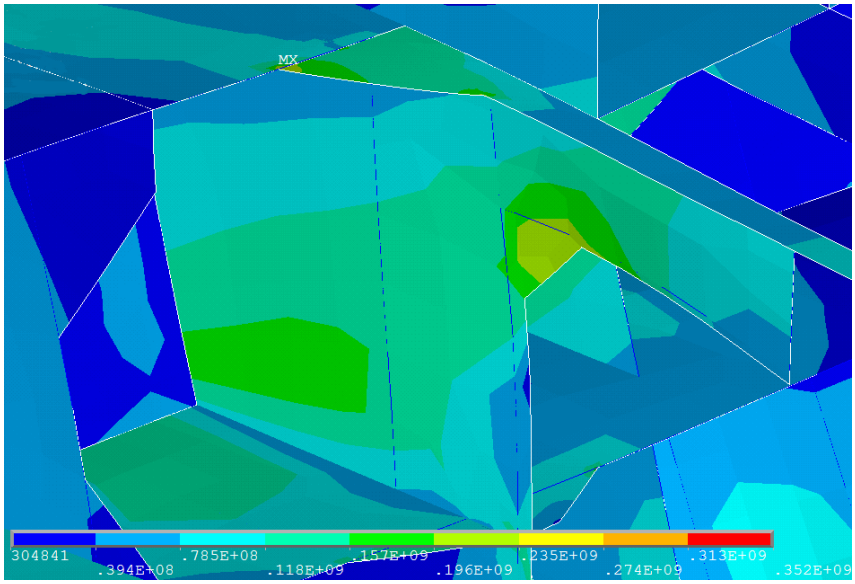

Figure 56: *von Mises stress* due to load case No. 6, ice belt region, cut off from boundary effects, zoom on stress concentration